AEDC-TR-70-90

Copy 2

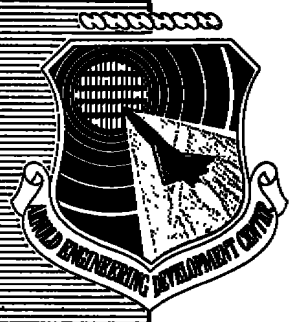

EXPERIMENTAL INVESTIGATION OF THE SCATTERING OF A MONOENERGETIC ARGON MOLECULAR BEAM FROM A SOLID ARGON SURFACE

M. R. Busby and R. F. Brown

ARO, Inc.

October 1970

VON KÁRMÁN GAS DYNAMICS FACILITY
ARNOLD ENGINEERING DEVELOPMENT CENTER
AIR FORCE SYSTEMS COMMAND
ARNOLD AIR FORCE STATION, TENNESSEE

NOTICES

When U. S. Government drawings specifications, or other data are used for any purpose other than a definitely related Government procurement operation, the Government thereby incurs no responsibility nor any obligation whatsoever, and the fact that the Government may have formulated. furnished, or in any way supplied the said drawings, specifications, or other data, is not to be regarded by implication or otherwise, or in any manner licensing the holder or any other person or corporation, or conveying any rights or permission to manufacture, use, or sell any patented invention that may in any way be related thereto.

Qualified users may obtain copies of this report from the Defense Documentation Center.

References to named commercial products in this report are not to be considered in any sense as an endorsement of the product by the United States Air Force or the Government.

EXPERIMENTAL INVESTIGATION OF THE SCATTERING OF A MONOENERGETIC ARGON MOLECULAR BEAM FROM A SOLID ARGON SURFACE

M. R. Busby and R. F. Brown
ARO, Inc.

FOREWORD

The research reported herein was sponsored by the Arnold Engineering Development Center (AEDC), Air Force Systems Command (AFSC), Arnold Air Force Station, Tennessee, and in support of Program Element 61102F.

The results of research were obtained by ARO, Inc. (a subsidiary of Sverdrup & Parcel and Associates, Inc.), contract operator of the AEDC, AFSC, under Contract F40600-71-C-0002. The research was conducted from November to December 1969 under ARO Project SW3003. The work described here is extracted from a larger effort by the primary author which satisfies the PhD dissertation requirements for the University of Tennessee Space Institute. The manuscript was submitted for publication on February 27, 1970.

The authors wish to thank Dr. J. D. Haygood, ARO, Inc., for his variance analysis of the experimental data.

This technical report has been reviewed and is approved.

Michael G. Buja
First Lieutenant, USAF
Research and Development Division
Directorate of Technology

Harry L. Maynard
Colonel, USAF
Director of Technology

ABSTRACT

An aerodynamic molecular beam and phase sensitive detection system were used to investigate the spatial distributions of argon atoms scattered from solid argon for: incident beam energies of 0.3 (T_o = 1400°K), 0.37 (1700°K), 0.43 (2000°K), and 0.5 ev (2300°K); incident angles (measured with respect to the surface normal) of 0 to 70 deg; and solid argon temperatures of 13.5°K. The effect of surface temperature on the distributions for 0.5-ev beams at 70-deg incidence was studied in the range from 13.5 to 23°K. Both in-plane and out-of-plane spatial distribution measurements were made, and highly nondiffuse supraspecular flux distributions were observed for the noncondensing atoms. The experimental data indicated that the angle of maximum reflected intensity was independent of the beam intensities, beam energies, beam incidence angles, and surface temperatures investigated; and its value was approximately 75 deg. The shape of the in-plane spatial distributions was essentially independent of the beam incidence angles and beam intensities studied. However, for increasing beam energies, the scattering distributions broadened. The out-of-plane distributions were broader than the corresponding in-plane lobes. The beam capture coefficient was a monotonically decreasing function as the angle of incidence and the incident beam energy increased. However, the capture coefficient of a 0.5-ev argon beam impinging at 70 deg increased as the surface temperature increased from 13 to 23°K.

CONTENTS

APPENDIXES

NOMENCLATURE

A	Maximum signal intensity for cosine distribution
C_b	Beam capture coefficient
E_i	Incident beam energy, ev
I_o	Incident beam intensity, molecules/sec-cm^2
$\vec{i}$	Incident beam unit vector
n_i	Total incident beam flux, molecules/sec
n_r	Total reflected beam flux, molecules/sec
n_t	Total gas flux leaving the surface
$\vec{n}$	Unit target normal vector
$\vec{r}$	Unit vector in the scattering direction
S	Detector signal, mv
T_o	Source stagnation temperature
T_s	Surface temperature, °K
ϕ	Out-of-plane or transverse plane angle
θ_i	In-plane or azimuthal angle (incident)
θ_r	In-plane or azimuthal angle (reflected)

SECTION I
INTRODUCTION

1.1 BASIC CONSIDERATIONS

The nature of the interaction at the gas-solid interface represents an extremely important but incompletely understood area of scientific inquiry. An understanding of gas-surface interaction processes is being sought by investigators in several fields. For example, a knowledge of the mechanism for the interaction of neutral, nonreacting gases with solid surfaces would serve the physical chemist investigating the complex processes of surface catalysis and would provide the physicist with information concerning the surface states of solids and gas-solid interatomic potentials. The aerodynamicist must ultimately interpret the aerodynamic forces on a vehicle traveling through a low-density atmosphere as well as the rate at which that atmosphere transports energy to the vehicle in terms of individual molecule-surface collisions. An understanding of the efficiency of cryogenic vacuum pumps is similarly linked to individual particle-surface interactions. Thus, detailed experimental observations of these interactions can lead to conclusions concerning the basic structure of both the surface and gas molecules. However, the understanding of the processes occurring at a gas-solid interface is much less developed than that pertaining to processes occurring in the bulk gas and solid phases. This is to be expected since knowledge of interface phenomena generally requires a higher level of understanding of the fundamental processes in the individual phases.

1.2 PREVIOUS EXPERIMENTAL SCATTERING STUDIES WITH MOLECULAR BEAMS

Early experiments with molecular beams reflected from surfaces were generally concerned with the observation of wave diffraction effects. Estermann and Stern (Ref. 1) observed diffraction maxima for hydrogen and helium on cleaved single crystals of lithium fluoride. In 1931 Zahl and Ellett (Ref. 2) reported flux distribution measurements in mercury beams after reflection from sodium chloride, potassium chloride, potassium bromide, and potassium iodide. Lobular reflection patterns were observed with the lobe maxima displaced from the specular direction. Heating the target and/or cooling the beam increased this displacement toward the surface normal. Reflection of this type is shown qualitatively in Fig. 1, which is a polar plot of reflected particle flux versus angle of reflection, θ_r, in the principal plane (i.e., defined by the incident beam axis and the surface normal).

Kellogg (Ref. 3) reported lobular reflection of thallium, lead, and antimony from cleaved sodium chloride crystals. Thallium and lead showed near-specular lobe maxima, whereas antimony showed a lobe displacement from the specular direction toward the target tangent. All beams were hot relative to the surface temperature. Similarly, Hancox (Ref. 4) obtained lobular scattering patterns of mercury and cadmium from lithium fluoride, lithium chloride, sodium fluoride, potassium iodide, and sodium chloride, and his results showed the same trends in the dependence of lobe direction on beam temperature, target temperature, and angle of incidence as reported by Zahl and Ellett.

The sensitivity of reflected beam flux measurements was greatly increased by modulating the molecular beam and passing the output signal from a mass spectrometer detector through a narrow band lock-in amplifier (Ref. 5). Smith and Fite (Ref. 6) used this technique to study the reflection of hydrogen and argon from polycrystalline nickel surfaces. The experimental results were nonspecular, lobular reflection patterns similar to those observed in earlier experiments with metallic vapor beams. These patterns were observed only in some cases depending on the target preparation, and for those cases the lobe maxima were either in the specular direction or shifted toward the normal.

Datz, et al. (Ref. 7), obtained nonspecular lobular reflections of heated and unheated helium and deuterium from platinum. Their variations in lobe position with beam temperature and angle of incidence agree qualitatively with those of Zahl and Ellett. Similar results were obtained by Hinchen and Foley (Ref. 8) for the scattering of argon, helium, nitrogen, and xenon from platinum ribbon. Prolonged heating of the ribbon produced the narrowest patterns, presumably because of growth in the crystallite size and the general perfection and healing of the crystallite surface.

Smith and Saltsburg (Ref. 9) obtained intense specular helium reflections and broad, nonspecular argon reflections from epitaxially grown gold films. Surface cleanliness was assured since the gold film was formed by vapor deposition at more than ten times the rate of arrival of background contaminant particles.

O'Keefe and French (Ref. 10) have obtained the scattered flux distributions of nearly monoenergetic high energy (0.25 to 2.0 ev) argon beams impinging upon a single crystal of tungsten. The peak intensities for all scatter patterns were found to lie below the specular angle and were narrower than the argon distributions found at lower energies. Adsorbed nitrogen or carbon monoxide on the target surface resulted in wider distributions and a shift of the maximum toward the surface.

More recently, Caldwell, Busby, and Brown (Ref. 11) reported lobular scattering patterns for 0.30 to 0.54 ev monoenergetic argon beams reflected from an engineering (undefined) copper surface. The variations in lobe position with beam temperature and angle of incidence agree qualitatively with those obtained from well-characterized surfaces for surface temperatures of 285 and 131°K. However, with a surface temperature of 77°K, only slightly lobular patterns were observed, and at 36°K the spatial distribution of the reflected beam was diffuse or cosine.

The experimental results indicate that there are many similarities in the scattering patterns of different gas-solid systems. It is indeed remarkable that these similarities should exist for several gases, e.g., the rare gases, metallic vapors, hydrogen, etc., on a wide variety of solids, e.g., ionic and metallic, monocrystalline and polycrystalline, with different lattice structure, surface preparations, impurities, and atomic masses. The main characteristics that are common to a majority of the scattering patterns have been summarized by Stickney (Ref. 12). Although one should not assume these characteristics to be universally true, they do, nevertheless, reflect the results of the existing experimental data prior to this work.

1.3 SIGNIFICANCE OF THE PRESENT WORK

Although large quantities of experimental scattering data have been and are being reported, a completely satisfactory general explanation of the results based on theoretical models of gas-surface interactions has yet to be established. A recurring theme in gas-surface interaction theory is that neither the physical properties of the collision partners nor the mechanisms of collision are sufficiently understood. Sometimes the investigator tries to determine the outcome of the interaction from basic molecular properties and lattice theory or to infer potential well depths or heats of adsorption by interpreting the results of interaction measurements.

The present study represents an attempt to improve the state of knowledge of the field of gas-surface interactions through a detailed experimental study of perhaps the most fundamental gas-solid system, i.e., the interaction of an element in the gaseous state with its own solid phase. It is only for such a system that the combination rules for the interatomic potential parameters (Ref. 13) can be applied with confidence. The interaction of a rare gas with its own solid phase, in particular for these studies of the argon-argon system, results in an uncontaminated surface because of the continuous partial capture of the incident monoenergetic molecular beam by the cryogenically cooled target substrate. Finally, the interaction of a monatomic, chemically inert gas on its own solid phase is the most easily modeled system from a theoretical point of view. The present study thus gives, for the first time, fundamental experimental data which can be used to test previous and contemporary theoretical models or to formulate new theories for the gas-solid interface phenomena.

In a series of preliminary investigations conducted by Busby and Brown (Ref. 14), it was found that rare gas-rare solid interaction experiments could be performed in the AEDC Aerodynamic Molecular Beam Chamber because of the high pumping capacity afforded by cryogenic cooling and the observation that the condensation rate of the incident molecular beam is initially very large but then decreases to a final steady-state value which allows a detectable signal. After a survey of the existing literature, it is evident that the results of the preliminary investigation (Ref. 14) of the scattered spatial distributions of argon reflected from its own solid were the first of their kind.

SECTION II
EXPERIMENTAL APPARATUS

2.1 AERODYNAMIC MOLECULAR BEAM CHAMBER

The aerodynamic molecular beam experimental test cell (Fig. 2) is a stainless steel cylinder, 3 ft in diameter by 6.5 ft in length, which is subdivided into three sections by two removable bulkheads. The first bulkhead separates the nozzle section of the cell from the collimation section and serves as a mounting base for the beam skimmer. The beam collimating orifice is mounted on the second bulkhead which separates the collimation and test sections of the cell. A complete description of the beam system and its performance has been previously described by Brown and Heald (Ref. 15).

2.1.1 Nozzle Section

Vacuum conditions are produced and maintained in the nozzle section by a 16-in. oil diffusion pump, a 20°K gaseous-helium-cooled cryoliner, and a 77°K liquid-nitrogen-cooled cryoliner. The total pumping speed for air is in excess of 500,000 liters per second. Operating pressures from 10^{-4} to 10^{-7} torr can be maintained in this section.

The aerodynamic molecular beam source (Fig. 3) is mounted in the nozzle section of the cell. The source is a 3/16-in.-diam by 8-in.-long tantalum tube bent in a U-shape and mounted in a water-cooled copper heat shield. The gas enters both ends of the source and effuses from a 0.0135-in.-diam orifice drilled through the 0.006-in. tube wall. The tantalum is resistance heated to temperatures of 2600°K, as measured with an optical pyrometer.

2.1.2 Collimation Section

Operating pressures of 10^{-7} torr are maintained in the collimation section by a 10-in. oil diffusion pump and the gaseous-helium and liquid-nitrogen-cooled cryoliners. The pumping speed for air is in excess of 350,000 liters per second in this section.

A small stream tube of the free-jet expansion in the nozzle section is separated from the general flow field by a cryogenically cooled skimmer located at the entrance of the collimation section. The skimmer is a hollow copper cylinder (Fig. 3) with a 1-in.-diam hole which allows passage of the gas into the section. Gaseous helium at 20°K is circulated within the cylinder which cryopumps a portion of the impinging free-jet expansion. The cooled skimmer virtually eliminates the interaction previously reported by Brown and Heald (Ref. 15). At the end of the collimation section a 4-mm-diam orifice aligned with the skimmer and nozzle orifice, collimates the gas stream so that a uniformly intense and monoenergetic molecular beam enters the test section.

2.1.3 Test Section

In the test section vacuum conditions are maintained by a 10-in. oil diffusion pump and the 20°K gaseous-helium and 77°K liquid-nitrogen-cooled cryoliners; the pumping speed for air is in excess of 110,000 liters per second. An operating pressure of 10^{-8} torr is easily attainable in this section. The test section contains the beam detection systems, the cryogenically cooled target, and their mounting and drive mechanisms.

2.2 DETECTION SYSTEMS

The use of molecular beams for atomic and molecular interaction experiments has resulted in the development of numerous beam detection techniques (Ref. 16). One technique which aids in the discrimination between the beam signal and background noise is to modulate the molecular beam at a convenient frequency and then by AC amplification measure only that part of the signal which has the proper frequency and phase. This is generally referred to as modulated beam or "lock-in" detection, and the

technique is described in detail in Refs. 5 and 17. The detector system described herein combines the beam modulation technique with a quadrupole mass spectrometer as the electrical signal source. The use of the mass spectrometer further increases the signal-noise ratio of the detector by rejecting all signals at mass numbers other than the beam mass number.

As depicted in Fig. 4, the molecular beam to be detected is chopped into pulses by two slots in a rotating wheel. These slots are 90-deg sectors cut out of a 2-in.-diam aluminum disk. The beam chopper is driven by a two-phase, synchronous vacuum-rated motor turning at 150 Hz. These beam pulses then pass into the ionization region of the quadrupole mass spectrometer which is tuned to the mass number of the beam molecules. The resulting ion current is amplified by an electron multiplier which sends a pulsed electrical signal to the Princeton Applied Research HR-8 "lock-in" amplifier. This amplifier operates as a narrow bandpass amplifier, the center frequency of which is adjusted to the chopping frequency. A light and photocell mounted at the chopper wheel generate a reference signal. The amplifier increases the signal-noise ratio by amplifying and detecting only the electrical signal at the exact frequency of the reference signal. The pulsed signal is rectified and integrated into a DC signal at the output of the "lock-in" amplifier. This signal is read out on a strip chart recorder, and an oscilloscope is used to monitor the AC tuning of the amplifier.

The detector was designed for two modes of operation: (1) as a molecular flow rate detector and (2) as a flow density detector. The mode of operation is determined by the manner in which the beam gas is introduced into the detector ionization region as shown in Fig. 5. As a molecular flow rate (beam intensity) detector, the beam must pass through the "steady-state" box before entering the ionization region of the mass spectrometer. Since the beam molecules are brought to equilibrium with the walls and the baffle of this box, the detector responds only to changes in molecular flow rate. All spatial flux distribution data were taken in this operational mode. The box is removable to permit use of the instrument as a flow density detector. In this configuration the beam pulses pass directly into the ionization region without striking any solid surface. Hence, changes in flow velocity change the density of the beam gas in the ionization region. All time-of-flight or beam energy measurements were taken in this operational mode.

This detection system has the capability of recovering beam intensity signals that are three orders of magnitude less than the background gas intensity. A complete description of the detectors and their performance has been given by Heald (Ref. 18).

The total beam flux is measured by utilizing a miniature ionization gage. The gage is enclosed in a glass envelope, but the normal 1-in.-diam opening was reduced to 6 mm in order to increase the directional sensitivity (Fig. 2).

2.3 TARGET AND DETECTOR MOVEMENT MECHANISMS

The target and its mount rotate about an axis perpendicular to the incoming beam (Fig. 6). Motion is accomplished by a variable speed-torque-motor chain-drive

combination. The position of the target is determined from a calibrated voltmeter readout which is produced from a ten-turn potentiometer connected to the chain drive. In-plane and out-of-plane motions (see Section III) were likewise provided by a torque-motor chain-drive combination (Fig. 6), and a potentiometer voltmeter system was used to determine the position of the detector. The geometry of motion as well as the alignment of the detection system will be discussed in detail later.

2.4 TARGET SUBSTRATE

The target substrate for these experiments was a copper disk hand-polished to a mirror finish with jeweler's rouge and rinsed with acetone. The disk is hollow so that gaseous helium can be circulated through it. The substrate temperatures were maintained by a Collins cryostat. Helium vapor pressure thermometers were used to measure target temperatures in the range of 13 to 30°K and Chromel®-constantan thermocouples in the range of 30 to 285°K.

SECTION III
DETECTOR MOVEMENT GEOMETRY AND COORDINATE SYSTEM

For a target-fixed coordinate system the incident beam unit vector, $\vec{i}$, is defined through an azimuthal angle, θ_i, measured from the unit target normal, $\vec{n}$. The plane containing $\vec{n}$ and $\vec{i}$ will be referred to as the "in-plane" or principal plane (Fig. 7); the intersection of this plane with the target face will be referred to as the principal axis. The transverse axis is perpendicular to the principal axis and also lies on the target face.

The geometry used to describe the reflected beam is shown in Fig. 8. The reflected or scattering direction is denoted by the unit vector $\vec{r}$. The detector lies along the vector $\vec{r}$. An "out-of-plane" or transverse plane is defined as that plane containing the transverse axis and the vector $\vec{r}$. Note that the transverse planes are always perpendicular to the principal plane. The line of intersection of a transverse plane with the principal plane makes an in-plane angle θ_r with the target normal $\vec{n}$ and an out-of-plane angle ϕ with the reflection vector $\vec{r}$. Since $\vec{r}$ is a variable, many transverse planes exist all passing through the single transverse axis. Properties displayed in planes of constant θ_r are transverse sections of the scattered beam, whereas a display of the properties in the plane $\phi = 0$ is a principal plane section of the scattered beam.

SECTION IV
EXPERIMENTAL PRE-TEST PROCEDURES

4.1 SYSTEM ALIGNMENT AND CALIBRATION

The alignment of the skimmer, collimator, target, and detector system was accomplished by use of a laser as a reference beam source. Following the calibration of the potentiometer voltmeter, the target could be positioned to within an estimated ±1 deg of arc, whereas the in-plane and out-of-plane angles were observed to be within an estimated ±1/2 deg of that indicated by a voltmeter reading. In addition to the electrical position indicator, reference position marks for the target and detector were made in the test section and were visually observed during these experiments as a check for the potentiometer calibrations.

4.2 EXPERIMENTAL TEST GAS

For these experiments ionization grade Matheson Gold Label Ultra-pure argon was used. The gas was analyzed with a mass spectrometer (Table I, Appendix II) and minimum purity was 99.999 percent.

4.3 BEAM CHARACTERISTICS

4.3.1 Intensity Cross-Section of the Argon Beam

Measurements were made with the miniature ionization gage to determine the intensity (molecules/sec-cm^2) at various points across the beam. A plate with 0.014-in.-diam hole was placed over the ionization gage opening and readings were taken at positions visually measured with a transit. As shown in Fig. 9, the beam distribution has a uniform core.

4.3.2 Argon Beam Energy Measurements

In order to measure the incident argon beam energy, the detector system was operated in its flow density or "fly-through" mode (Fig. 5). The velocity distributions for a constant source pressure (800 torr) and variable source temperatures were obtained. The experimental apparatus and data acquisition procedures have been described in detail by Powell and Heald (Ref. 19). The reduction of the velocity distribution data is comprehensively and completely discussed by Benek, Busby, and Powell (Ref. 20). The normalized data and the corresponding "best fit" theoretical distribution for a heated argon beam are shown in Fig. 10. Beam energies determined from the velocity distribution data and their corresponding tantalum source temperatures are presented in Fig. 11. The source temperatures were measured with an optical pyrometer, and it was assumed throughout these experiments that a given pyrometer reading would be accurately indicative of the corresponding beam energy.

The argon molecular beam used in these experiments is a monoenergetic aerodynamic molecular beam. Aerodynamic beams differ from classical oven or Maxwellian beams in several areas: (1) the intensity is greater, (2) the mean energy is higher, and (3) the velocity distributions are very narrow. The term monoenergetic is applied since at Mach 20, for example, the velocity distribution of an aerodynamic beam is such that 80 percent of the beam molecules have a velocity that is within five percent of the mean velocity (Ref. 21).

4.3.3 Argon Beam Performance

Argon beam performance data were obtained by lowering the miniature ionization gage into the beam and obtaining the gage reading as the source pressure and temperature were varied over the desired range (Fig. 12). Previous calibration with an oven beam source has shown that, if the ionization pressure gage reading for argon is multiplied by 2.5×10^{20}, the result is the total beam flux in molecules per second.

The source pressure was maintained such that polymerization in the incident beam would not occur during these experiments. Experimental data relating to the onset of polymerization in argon beams for various source pressures and temperatures have been discussed by Ruby (Ref. 22). However, the data presented for this investigation are only for argon atoms.

4.4 VARIATIONS IN DETECTOR SYSTEM SENSITIVITY

The variation of the detector sensitivity with time was determined in the following manner:

1. An incident argon beam of known intensity and energy was scattered from the 285°K copper target.
2. The detector was positioned at the target normal and all the electronics were activated.
3. The reflected molecule signal was maximized, and its value recorded as a function of time (Fig. 13).

After four hours of operation, the signal magnitude remained nearly constant as time increased. The variation of the signal was due primarily to a loss in sensitivity with time of the magnetic strip electron multiplier used in the phase sensitive detection system. The effects of sensitivity variations on data acquisition will be discussed later.

4.5 TEST SECTION BACKGROUND PRESSURE

A mass spectrometer scan of the background gases in the test section revealed that water was the primary background constituent. The partial pressure of water was estimated to be 5×10^{-9} torr which corresponds to a strike rate of 2.4×10^{12} molecules/sec-cm^2. A typical experimental argon beam intensity is 1.2×10^{16} molecules/sec-cm^2, and thus water accounts for 0.02 percent of the total number of molecules striking a square centimeter of target per second. For all experimental tests the total background gas pressure was in the range of 1.2 to 1.8×10^{-8} torr.

SECTION V
EXPERIMENTAL PROCEDURE

The specific experimental procedures were as follows:

1. The beam flux was adjusted to its desired value.
2. The phase-sensitive detection system electronics were activated and adjusted to give the maximum reflected argon signal.
3. The Collins cryostat was activated and the cooling of the copper target was started.

4. The target was positioned to provide the desired angle of incidence.

5. When the detection system sensitivity was nearly constant (approximately four hours from the initial start-up) and the target temperature was 36°K, the spatial distribution of the reflected argon molecules was recorded (Fig. 14). The incident argon beam energy was 0.06 ev (corresponding to 285°K source conditions), and its intensity was 1.24×10^{16} molecules/sec-cm^2. These data provided a reference for the performance of the detector system as argon does not condense on a 36°K surface and the reflected spatial distributions are diffuse or cosine.

6. Having obtained the reference distribution, the target temperature was lowered. At approximately 30°K the beam molecules began to condense. This phenomenon was not investigated in detail, but the data indicate that at first the condensation rate was very large, then decreased, and finally reached a steady-state value. The data reported herein were obtained after the condensation rate had reached a steady-state value. During these experiments, the solid argon target surface was prepared by the partial condensation of the impinging argon molecular beam on the cryogenically cooled copper substrate. The surfaces were deposited by beams having various angles of incidence and at both constant and continuously varying substrate temperatures. The experimental scattering data were not affected by any of these surface preparation conditions provided steady-state conditions were attained prior to data collection. The crystallographic structure of the argon cryodeposits is unknown. Because of the difficulties associated with growing large crystals of argon (Ref. 23), the cryodeposit is most probably polycrystalline or amorphous. During these experiments, the solid argon target surface was continuously deposited and therefore "clean" but undefined.

7. Spatial distribution data for the argon atoms scattered from solid argon for various beam incidence angles and energies and various surface temperatures were recorded. Measurements were made in both the principal plane and transverse planes.

8. At the end of a set of experimental runs, the copper substrate was warmed and the argon cryofrost evaporated. A 0.06-ev argon beam was then scattered from the 36°K copper substrate, and the resulting cosine distribution was recorded. A comparison (Fig. 14) of this distribution with the one initially recorded revealed any changes in the detector system sensitivity. The use of these reference cosine distributions for a data error analysis and the estimation of a beam capture coefficient will be discussed later.

SECTION VI
EXPERIMENTAL RESULTS

6.1 GENERAL FEATURES OF THE SCATTERING PATTERNS

The data presented in this section are representative samples chosen to show the effects of the experimental parameters, e.g., angle of incidence, θ_i, incident energy, E_i, surface temperature, T_s, on the scattered beam spatial distributions. Also, for these sample sets only a representative subset of data is presented, in particular, data in two specific planes. With reference to the coordinate system in Fig. 8, these planes are:

1. the principal plane, ($\phi = 0$)
2. The transverse lobal plane ($\theta_r = \theta_{rm}$)

The angle θ_{rm} refers to the position in the principal plane where the reflected intensity is a maximum. In-plane scattering is displayed in the principal plane, and out-of-plane scattering is presented by way of the transverse lobal plane. A photograph of a three-dimensional model of a typical scattering distribution is shown in Fig. 15.

6.2 EFFECTS OF PARAMETER VARIATIONS

The effects of variations in incidence angle, incident intensity, incident energy, and surface temperature will now be presented for sets of data covering the range over which θ_i, I, E_i, and T_s were varied during the experiments.

6.2.1 Variation of Beam Intensity

The in-plane scattering distributions of a 0.5-ev argon beam impinging at 60 deg on a 13.5°K argon cryosurface are displayed in Fig. 16. Since all other experimental tests were conducted with a beam intensity, I_o, of 1.24×10^{16} molecules/sec-cm^2, it was necessary to determine the variation in the scattered distributions as a function of intensity. Thus, values of $2I_o$, I_o, $(1/2)I_o$, and $(1/3)I_o$ were set and upon normalizing* the spatial distribution data (Fig. 17), there was no detectable variation with beam intensity. Similar results were obtained for the out-of-plane data.

6.2.2 Variation of Beam Incidence Angle

The in-plane scattering distributions of a 0.5-ev argon beam impinging upon a 13.5°K solid argon surface are presented in Fig. 18. For each angle of incidence the angle of maximum reflected intensity, θ_{rm}, was approximately 75 deg. It is obvious that the condensation rate or capture coefficient of the incident beam increases significantly as the incidence angle measured with respect to the target normal decreases. However, if the in-plane data of Fig. 18 are normalized, there is no appreciable difference in the shape of the reflected distribution (Fig. 19).

*The experimental data in this report are normalized to the maximum reflected intensities of the corresponding spatial distributions.

A comparison of the reflected flux in the principal and transverse planes for various incidence angles reveals that the out-of-plane lobes are broader than their corresponding in-plane lobes (Fig. 20). Also, normalizing the transverse lobal plane data, one concludes that the out-of-plane distributions become broader as the incidence angle decreases (Fig. 21).

6.2.3 Variation of Beam Incidence Energy

Complete sets of in-plane scattering data for an argon beam at various incidence energies striking a 13.5°K argon cryofrost are presented in Figs. 22, 23, 24, and 25 for θ_i equal to 70, 60, 45, and 30 deg, respectively. The spatial distribution for normal incidence is shown in polar coordinates (Fig. 26) in order to emphasize the symmetry of the scattering. For all cases studied, the angle of maximum reflected intensity, θ_{rm}, was approximately 75 deg and thus was independent of beam incidence energies. However, a decrease of beam energy at a fixed incident angle significantly increases the condensation rate or capture coefficient of the incident beam on the cryosurface. In addition, normalization of the in-plane data indicates that the shape of the scattering distribution broadens as the beam energy increases (Fig. 27).

6.2.4 Variation of Surface Temperature

The in-plane scattering distributions of a 0.5-ev argon beam impinging at 70 deg on 13, 18, and 23°K solid argon surfaces are shown in Fig. 28. For the surface temperatures studied, the angle of maximum reflected intensity was approximately 75 deg, indicating that θ_{rm} is independent of T_s in the range from 13 to 23°K. Also, the capture coefficient increases as the surface temperature increases over the range studied. These data were very difficult to obtain because of problems in maintaining the target substrate at the desired constant temperature.

6.3 AUXILIARY EXPERIMENTS

6.3.1 Krypton-Argon Scattering Experiment

Since the sublimation energy of solid argon (0.08 ev) is considerably less than the mean energy of the beam used in these experiments, sputtering, i.e., the ejection of surface atoms by the excess energy transfer of the impinging beam atoms, of the argon cryodeposit is possible. However, as reported in Ref. 14, argon beams at various angles of incidence and energies were not observed to sputter carbon dioxide (sublimation energy ~ 0.256 ev) or nitrogen (sublimation energy ~ 0.06 ev) cryodeposits.

A somewhat more definitive experiment was carried out during these tests, namely, the interaction of a 0.5-ev krypton beam on a slowly evaporating argon cryofrost. The mass ratio of krypton to argon is approximately two, and thus if krypton does not sputter argon then it is implied that argon does not sputter argon. The experimental results are shown in Fig. 29. The evaporating argon signal was recorded and periodically the krypton beam was allowed to strike the surface. Spikes in the argon signal would have been observed if sputtering were a predominant interaction mechanism.

However, no argon spikes were observed. The decrease in the argon signal (after initial krypton impingement) was due to the condensation of the krypton on the solid argon. Thus, the reflected argon spatial distributions are due to scattering of the incident gas beam from the solid argon surface rather than sputtering.

6.3.2 Surface History Experiments

The effect of surface history on the scattered flux distributions was considered during these tests. As previously stated in the experimental procedures, argon surfaces were prepared by impinging beams at various angles of incidence and energies and for constant and continuously varying surface temperatures. The effect of warming the cryodeposit and then cooling it to its original temperature was studied. There was no observable effect of the surface history on the reflected argon distributions if steady-state conditions were attained prior to data collection.

6.4 VARIANCE ANALYSIS OF THE EXPERIMENTAL DATA

Reference cosine distributions were taken at the beginning and end of each set of experimental runs. In addition, several in-plane lobular check runs were made for each set of experimental conditions. These tests provided the basis for the error analysis of the data. A variance analysis utilizing the t test (Ref. 24) was applied to the data. No significant differences were found for the assumed cosine distributions at the 95-percent confidence level. The maximum estimated error for the lobular distributions calculated by the t test was 4 percent at the 95-percent confidence level.

SECTION VII
CAPTURE COEFFICIENT

7.1 DEFINITION AND CALCULATION PROCEDURE FOR THE BEAM CAPTURE COEFFICIENT

The beam capture coefficient has been defined previously by Heald and Brown (Ref. 25) as

$$C_b = 1 - \dot{n}_r/\dot{n}_i$$

where $\dot{n}_r$ is the total reflected beam flux (molecules/sec) and $\dot{n}_i$ is the total incident beam flux. If any gas is evaporating from the target surface, the magnitude of the evaporation flux can be determined by extinguishing the incident beam and recording the remaining detector signal. Thus, the reflected beam flux is the difference between the total gas flux leaving the surface, $\dot{n}_t$, and the evaporation flux. In these experiments the surface temperatures were such that the evaporation flux was not detectable. Therefore, the beam capture coefficient is

$$C_b = 1 - \dot{n}_t/\dot{n}_i$$

The phase sensitive detection system responds to the number of particles per area per time, and thus the total reflected beam flux may be determined from the relation

$$\dot{n}_t \propto \int_{\Omega} S(\theta_r, \phi)\, d\Omega$$

where $S(\theta_r,\phi)$ is the detector signal, $d\Omega$ is the solid angle subtended by the detector, and θ_r and ϕ are the angles defined in Fig. 8. The detector solid angle in terms of the previously described coordinate system is

$$d\Omega = \cos\phi\, d\phi\, d\theta_r$$

The total incident argon flux, n_i, is determined from the reference cosine distribution of the noncondensing beam on the 36°K copper substrate. Thus, n_i may be analytically determined since for a cosine distribution $S(\theta_r,\phi) = A \cos\theta_r \cos\phi$ for the coordinate system of Fig. 8, i.e.,

$$\dot{n}_i \propto 4 \int_0^{\frac{\pi}{2}} \int_0^{\frac{\pi}{2}} A \cos\theta_r \cos^2\phi\, d\phi\, d\theta_r = \pi A$$

where A is the maximum signal intensity for the cosine distribution. The beam capture coefficient is expressed as

$$C_b = 1 - \frac{2}{\pi A} \int_0^{\frac{\pi}{2}} \int_0^{\frac{\pi}{2}} S(\theta_r, \phi) \cos\phi\, d\phi\, d\theta_r$$

The integral expression was evaluated by a double integral Simpson's rule on a digital computer. Transverse scattering plane data were recorded at 5-deg increments of θ_r over the range of 30 to 90 deg. In each of the transverse planes, 5-deg increments of ϕ were taken over the range of 0 and 45 deg. Thus, the three-dimensional lobular scattering patterns were placed on a grid of mesh size 5 x 5 deg. However, atoms scattered into regions of $\theta_r < 30$ deg and $\phi > 45$ deg were neglected since their contribution to the capture coefficient was assumed to be negligible.

7.2 VARIATION OF BEAM INCIDENCE ANGLE

The variation of argon beam capture coefficient with angle of incidence is presented in Fig. 30 for various incident beam energies. For all beam energies the capture coefficient is a monotonically decreasing function as the incidence angle increases; e.g., C_b varies from approximately 0.99 to 0.50 as θ_i increases from 0 to 70 deg for an incident beam energy of 0.50 ev. As θ_i approaches zero, the capture coefficient is near unity for all beam energies studied, indicating that energy transfer between the impinging atoms and the argon surface is very efficient.

7.3 VARIATION OF BEAM INCIDENCE ENERGY

In Fig. 31 the variation of the capture coefficient with beam incidence energy is shown for various angles of incidence and an argon surface temperature of 13.5°K. For

all angles of incidence the capture coefficient is a monotonically decreasing function as the beam energy increases, e.g., for θ_i = 70 deg C_b varies from approximately 0.83 to 0.50 as E_i increases from 0.30 to 0.50 ev.

7.4 VARIATION OF SURFACE TEMPERATURE

The variation of the capture coefficient of a 0.5-ev argon beam impinging at 70 deg on a variable temperature argon surface is presented in Fig. 32. The capture coefficient increases slowly with increasing surface temperature. However, the C_b versus T_s curve must reach a maximum at a $T_s \geq 23°K$ since the capture coefficient is essentially zero at a surface temperature of 36°K.

SECTION VIII
CONCLUDING REMARKS

The results of a detailed experimental investigation of the three-dimensional scattered flux distributions of a monoenergetic argon molecular beam scattered from its own solid phase have been presented. The characteristic trends of the experimental data may be summarized as follows:

1. The angle of maximum reflected intensity, θ_{rm}, was constant and independent of the beam intensities, beam energies, beam incidence angles, and surface temperatures investigated. Its value was approximately 75 deg.

2. The shape of the in-plane spatial distributions was independent of the beam incidence angles and beam intensities investigated. However, for increasing beam energies, the scattering distributions broadened.

3. The transverse lobal plane distributions were broader than the corresponding principal plane lobes.

4. The beam capture coefficient is a monotonically decreasing function as the angle of incidence and beam incidence energy increases.

5. The capture coefficient of a 0.5-ev argon beam impinging at 70 deg increases in the surface temperature range from 13 to 23°K.

There have apparently been no previous experimental studies of the spatial distributions of a rare gas reflected from its own solid. A discussion of the application of a theoretical model to these data will be presented in a companion report.

REFERENCES

1. Estermann, I. and Stern, O. "Diffraction of Molecular Rays." Zeits. f. Physik, Vol. 61, 1930, pp. 95–125.

2. Zahl, H. A. and Ellett, A. "Reflection of Mercury from Alkali Halide Crystals." Phys. Rev., Vol. 38, 1931, p. 977.

3. Kellogg, J. N. B. "Reflection of Thallium, Lead, and Antimony Atoms from Sodium Chloride Crystals." Phys. Rev., Vol. 41, 1932, p. 635.

4. Hancox, R. R. "Reflection of Metallic Atoms from Alkali Halide Crystals." Phys. Rev., Vol. 42, 1932, p. 864.

5. Fite, W. L. and Brackmann, R. T. "Collisions of Electrons with Hydrogen Atoms. I. Ionization." Phys. Rev., Vol. 112, 1958, p. 1141.

6. Smith, J. N., Jr. and Fite, W. L. "Recent Investigations of Gas-Surface Interactions Using Modulated Atomic Beam Techniques." Proc. 3rd Int. Symp. on Rarefied Gas Dynamics, Vol. 1, Academic Press, New York, 1963, p. 430.

7. Datz, S., Moore, G. E., and Taylor, E. H. "The Reflection of Modulated Helium and Deuterium Molecular Beams from Platinum Surfaces." Proc. 3rd Int. Symposium on Rarefied Gas Dynamics, Vol. 1, Academic Press, New York, 1963, p. 347.

8. Hinchen, J. J. and Foley, W. M. "Scattering of Molecular Beams by Metallic Surfaces." Proc. 4th Symposium on Rarefied Gas Dynamics, Vol. II, Academic Press, New York, 1966, p. 505.

9. Smith, J. N., Jr. and Saltsburg, N. "Atomic Beam Scattering from Epitaxially Grown Gold Films." J. Chem. Phys. Vol. 40, 1964, p. 3585.

10. O'Keefe, D. R. and French, J. B. "High Energy Scattering of Inert Gases from Well Characterized Surfaces. I. Experimental." Proc. 6th Symp. on Rarefied Gas Dynamics. Vol. 2, Academic Press, New York, 1969, p. 1279.

11. Caldwell, R. L., Busby, M. R., and Brown, R. F. "Spatial Distributions of 285 to 2500°K Argon Beams Scattered from an Undefined Copper Surface at Temperatures Between 36 and 285°K." AEDC-TR-69-142 (AD698325), December 1969.

12. Stickney, R. E. "Atomic and Molecular Scattering from Solid Surfaces." Advances in Atomic and Molecular Physics (D. R. Bates and I. Esterman) editors, Vol. 3, Academic Press, New York, 1967, p. 186.

13. Hirschfelder, J. R., Curtiss, C. F., and Bird, R. B. Molecular Theory of Gases and Liquids. John Wiley and Sons, Inc., New York, 1954, p. 168.

14. Busby, M. R. and Brown, R. F. "Preliminary Investigation of the Interaction of 0.30 to 0.54-ev Gaseous Argon with a Solid Argon Surface." AEDC-TR-69-195 (AD696106), November 1969.

15. Brown, R. F. and Heald, J. H., Jr. "Performance of an Aerodynamic Molecular Beam Chamber for Cryopumping and Adsorption Pumping Studies." Journal of Spacecraft and Rockets, Vol. 4, No. 4, 1967, pp. 476-480.

16. Trischka, J. W. Methods of Experimental Physics 3: Molecular Physics. Ed. by D. Williams, Academic Press, New York, New York, 1962.

17. Fite, W. L. and Datz, S. "Chemical Research with Molecular Beams." Annual Review of Physical Chemistry. Annual Reviews, Inc., Stanford, California, Vol. 14, 1963, pp. 61-68.

18. Heald, J. H., Jr. "Performance of a Mass Spectrometric Modulated Beam Detector for Gas-Surface Interaction Measurements." AEDC-TR-67-35 (AD648984), March 1967.

19. Powell, H. M. and Heald, J. H., Jr. "A System for the Measurement of Velocity Distributions of Molecular Beams." AEDC-TR-68-151 (AD675306), September 1968.

20. Benek, J. A., Busby, M. R., and Powell, H. M. "A Technique for the Analysis and Computerized Data Reduction of Velocity Distributions of Free Jet Expansions." AEDC-TR-70-84, to be published.

21. Anderson, J. B., Andres, R. R., and Fenn, J. B. "Supersonic Nozzle Beams." Advances in Chemical Physics. J. Ross, ed., Vol. 10, John Wiley and Sons, Inc., New York, 1966, pp. 275–318.

22. Ruby, E. C. "Measurements of the Concentration and Velocity Distributions of Clusters in Free Jet Expansions of Argon." University of Tennessee Space Institute Thesis, December 1968.

23. Peterson, O. G., Batchelder, D. N., and Simmons, R. O. "X-ray Diffraction Study of Argon Crystal Growth." Journal of Applied Physics, Vol. 36, 1965, p. 2682.

24. Youden, W. J. Statistical Methods for Chemists. John Wiley and Sons, Inc., New York, 1951, pp. 50–58.

25. Heald, J. H., Jr. and Brown, R. F. "Measurements of Condensation and Evaporation of Carbon Dioxide, Nitrogen, and Argon at Cryogenic Temperatures Using a Molecular Beam." AEDC-TR-68-110 (AD674596), September 1968.

APPENDIXES

I. ILLUSTRATIONS

II. TABLE

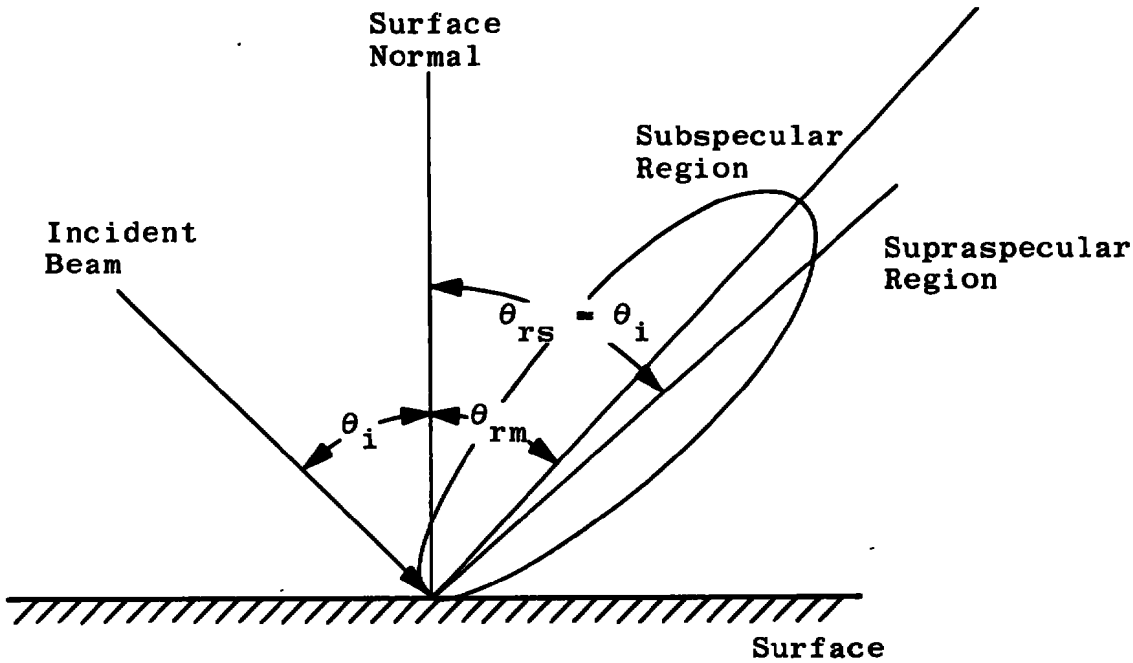

θ_i = Incident Beam Angle

θ_{rs} = Angle for Specular Reflection = θ_i

θ_{rm} = Angle of Maximum Reflected Intensity

Fig. 1 Nonspecular Lobular Reflection

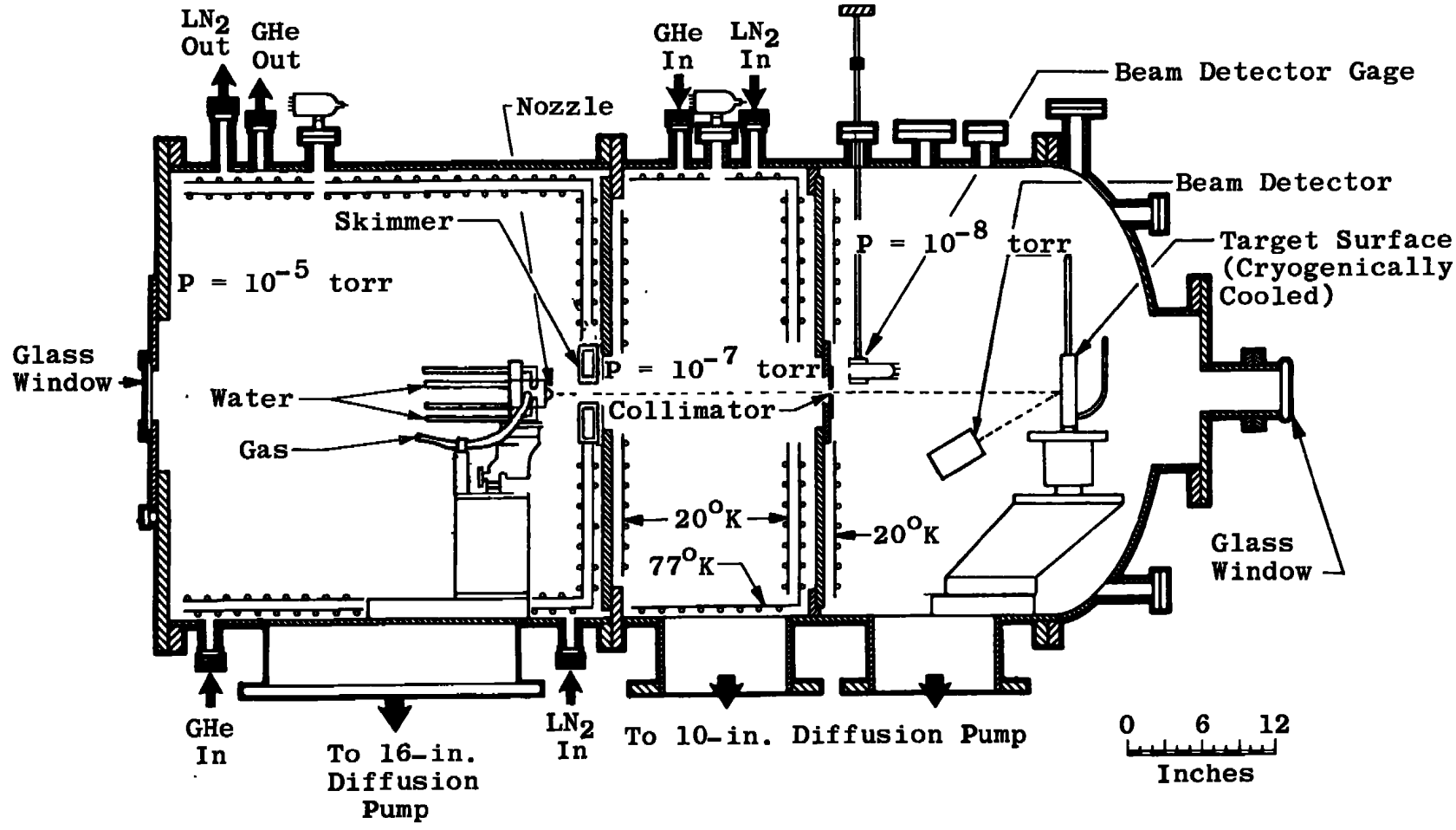

Fig. 2 Aerodynamic Molecular Beam Chamber

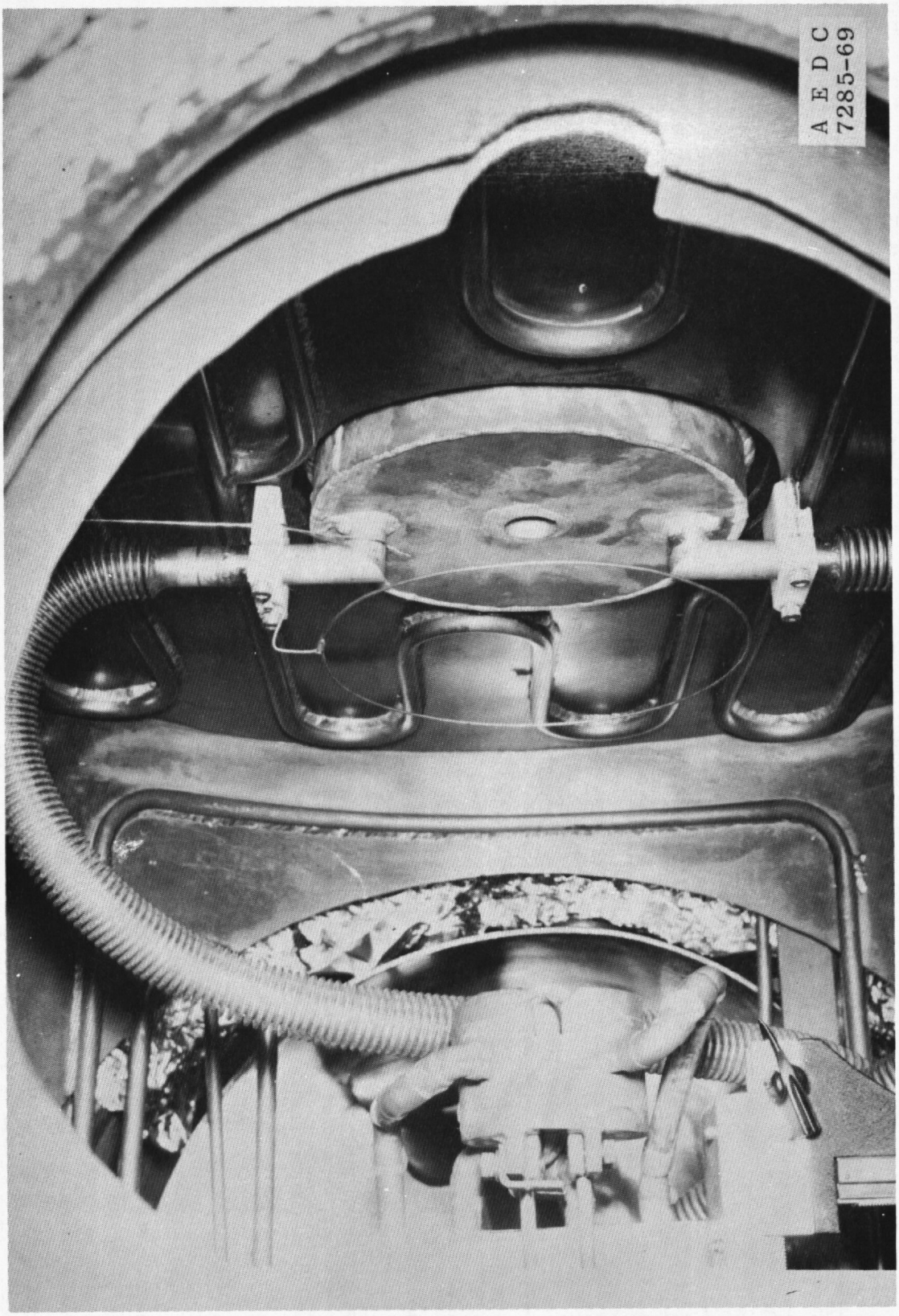

Fig. 3 Tantalum Gas Source and Cryogenically Cooled Skimmer

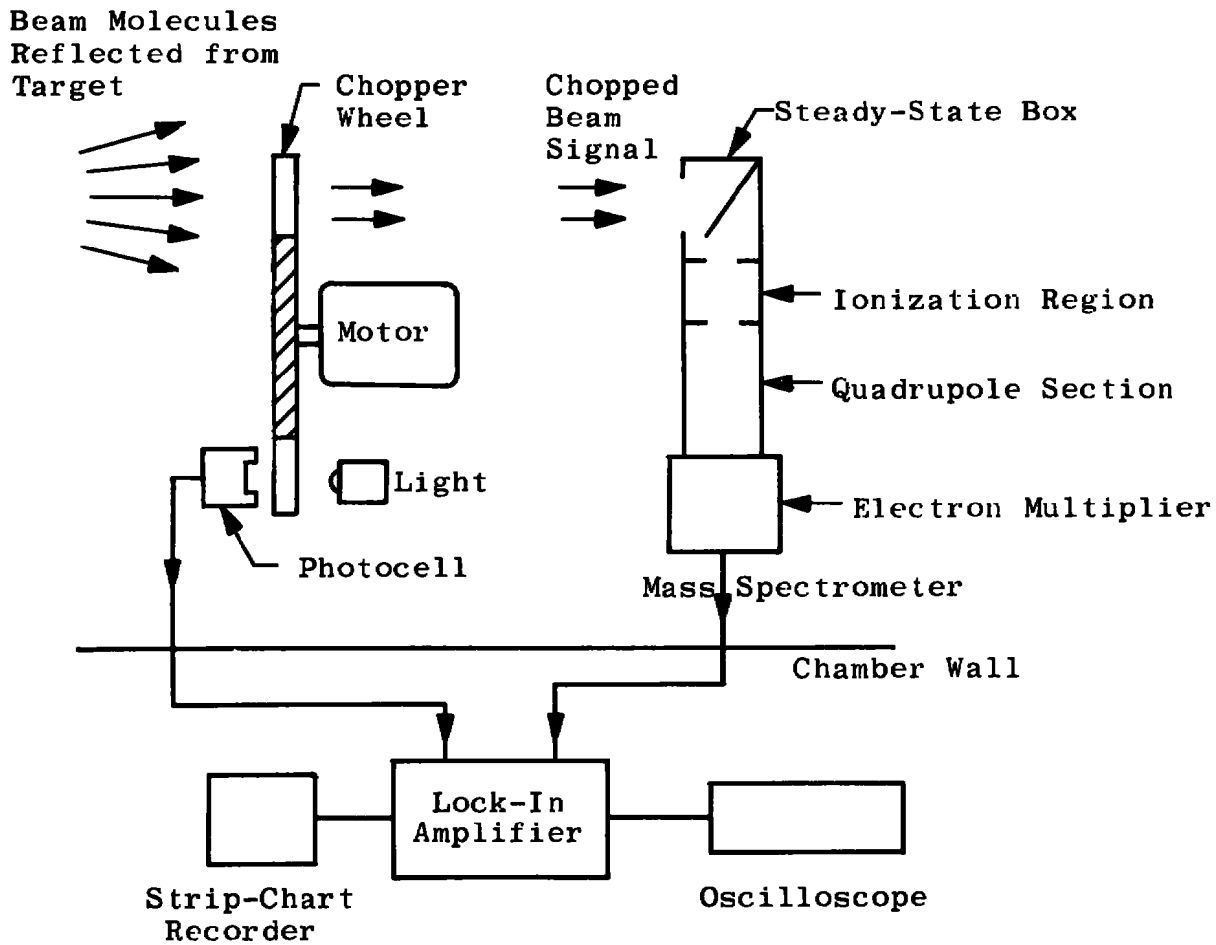

Fig. 4 Mass-Spectrometric Modulated Beam Detector

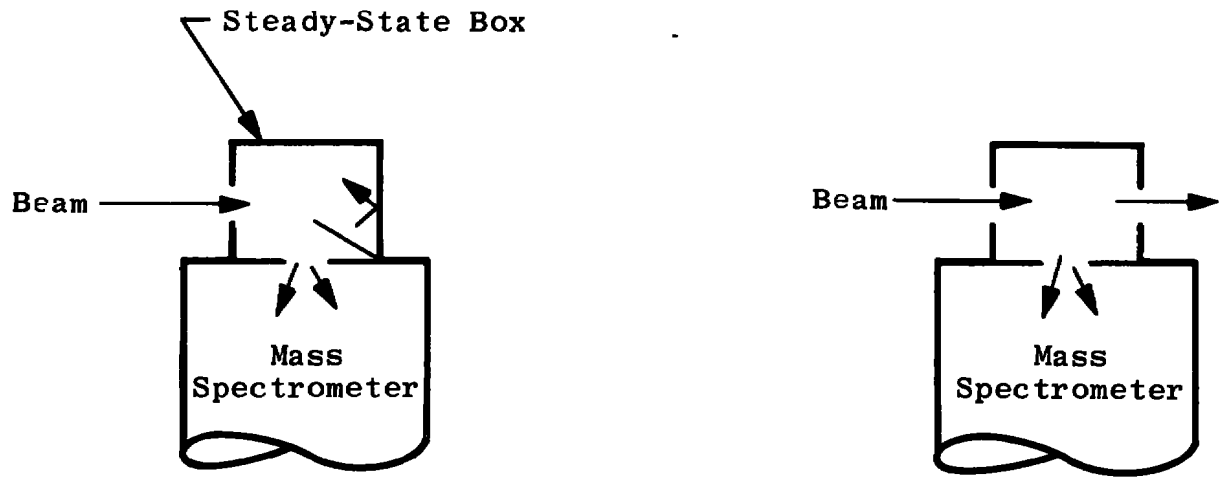

a. Molecular Flow Rate Detector

b. Molecular Flow Density Detector

Fig. 5 Operational Modes of the Detector

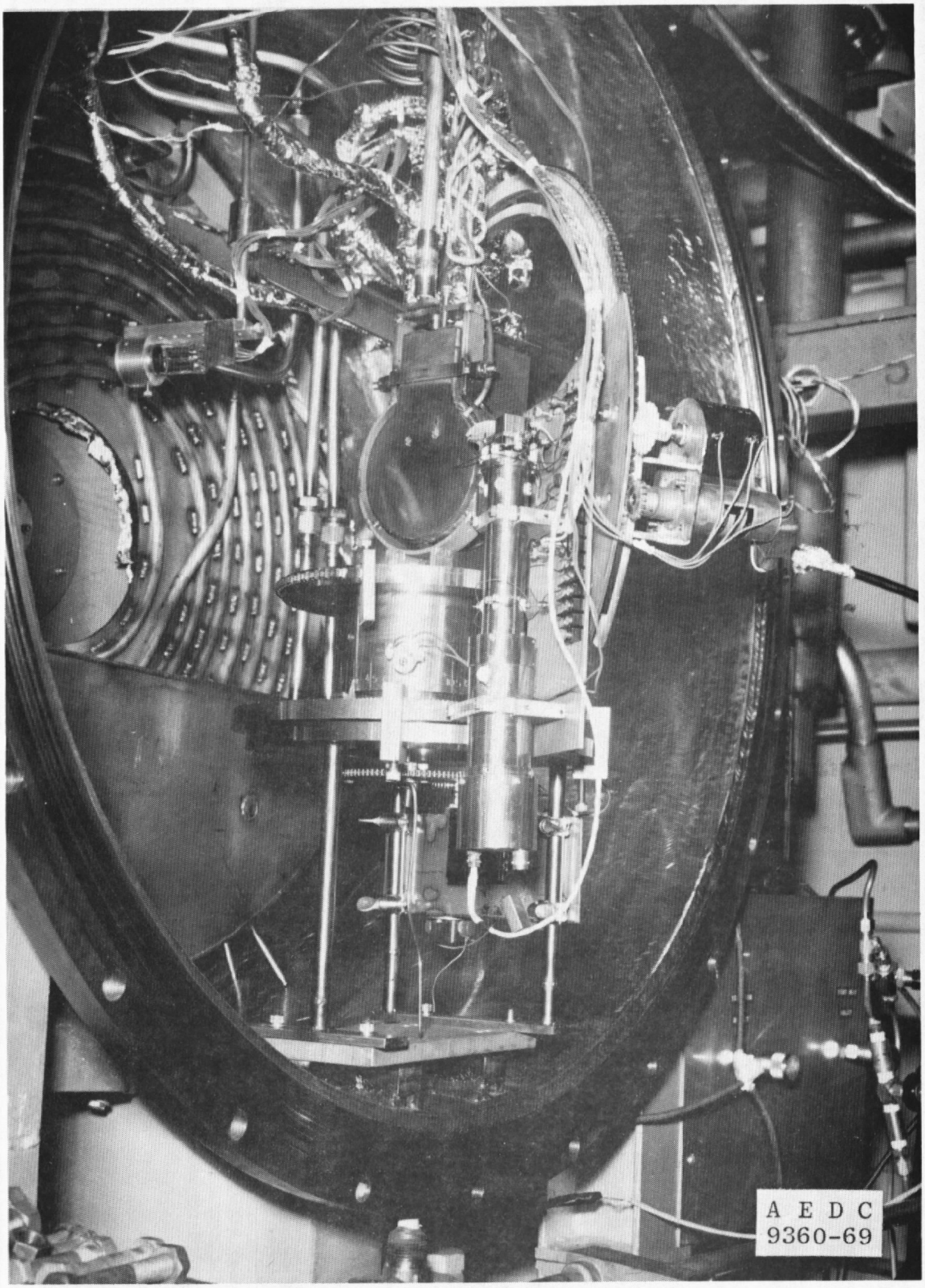

Fig. 6 Target and Detector Movement Mechanisms

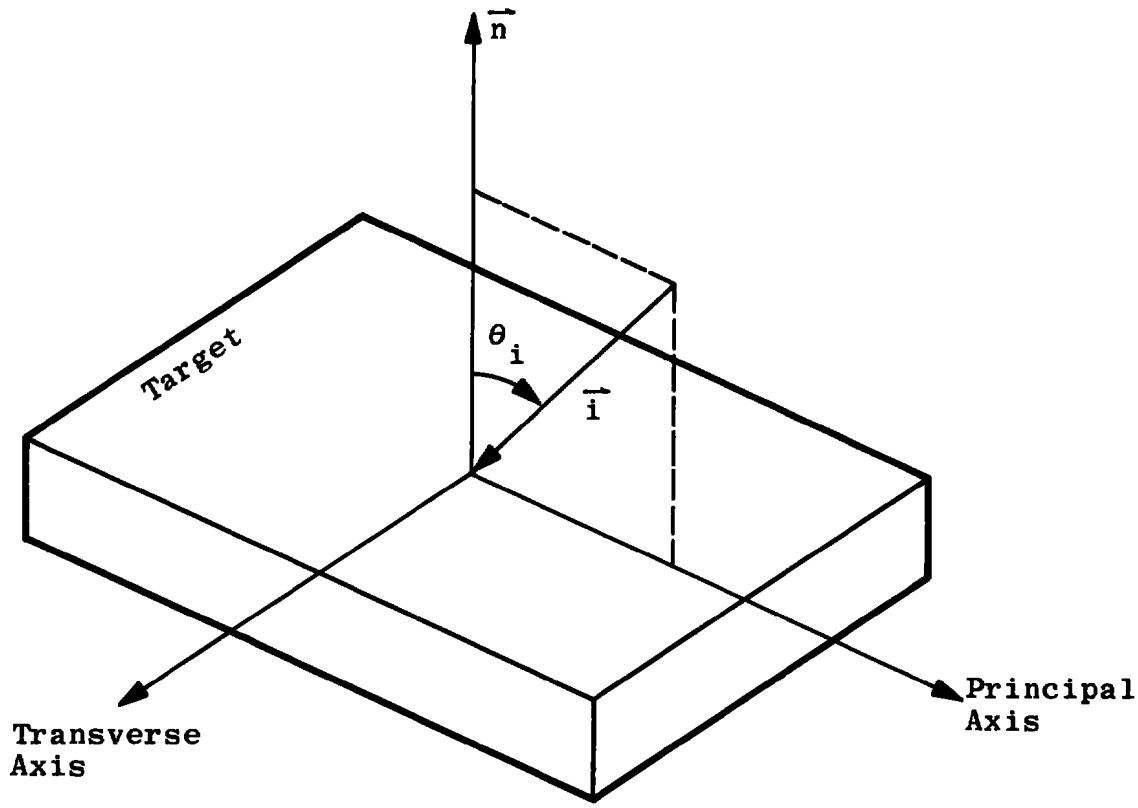

Fig. 7 Orientation Parameters for the Incident Beam

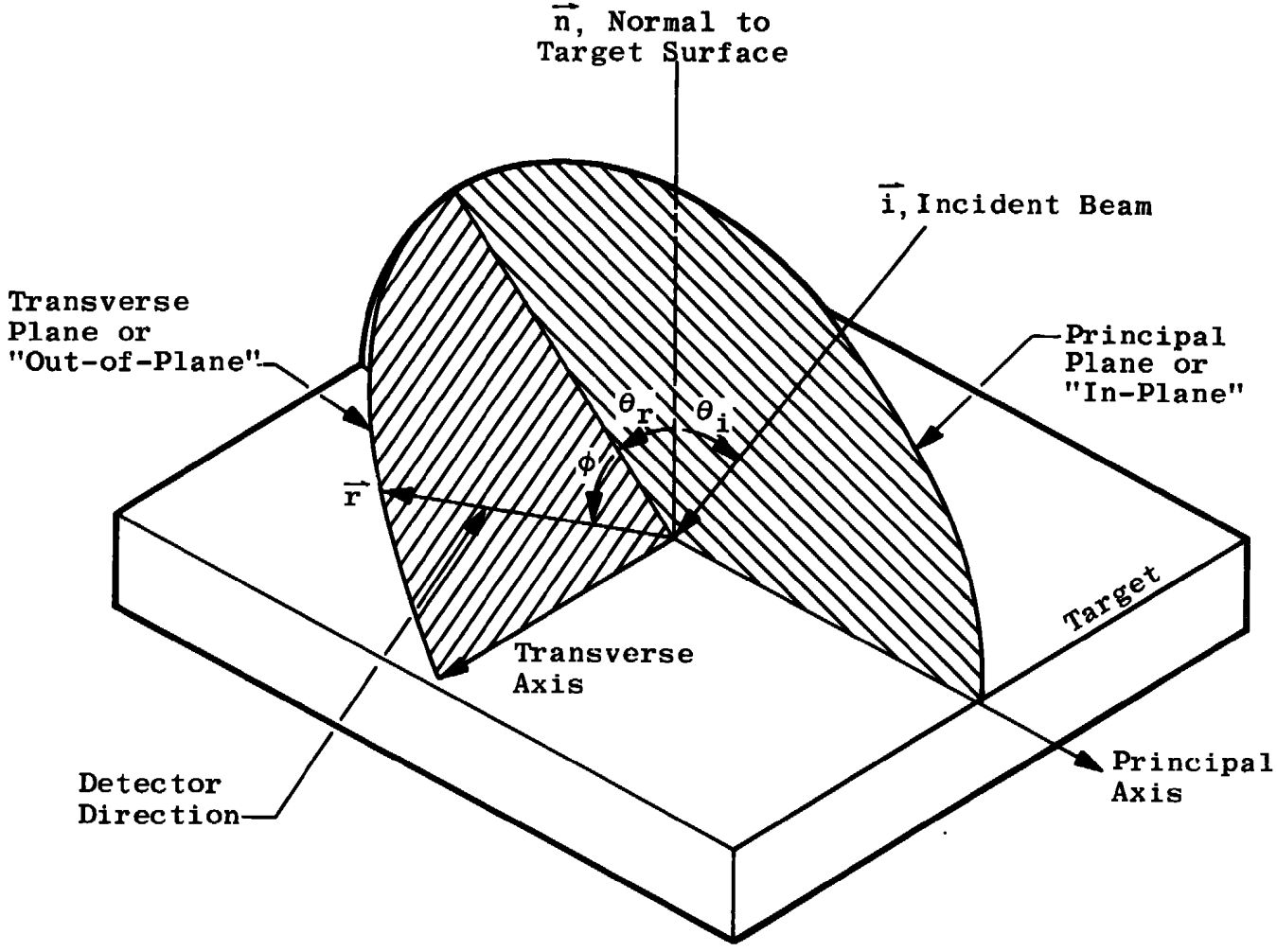

Fig. 8 Orientation Parameters for the Reflected Beam

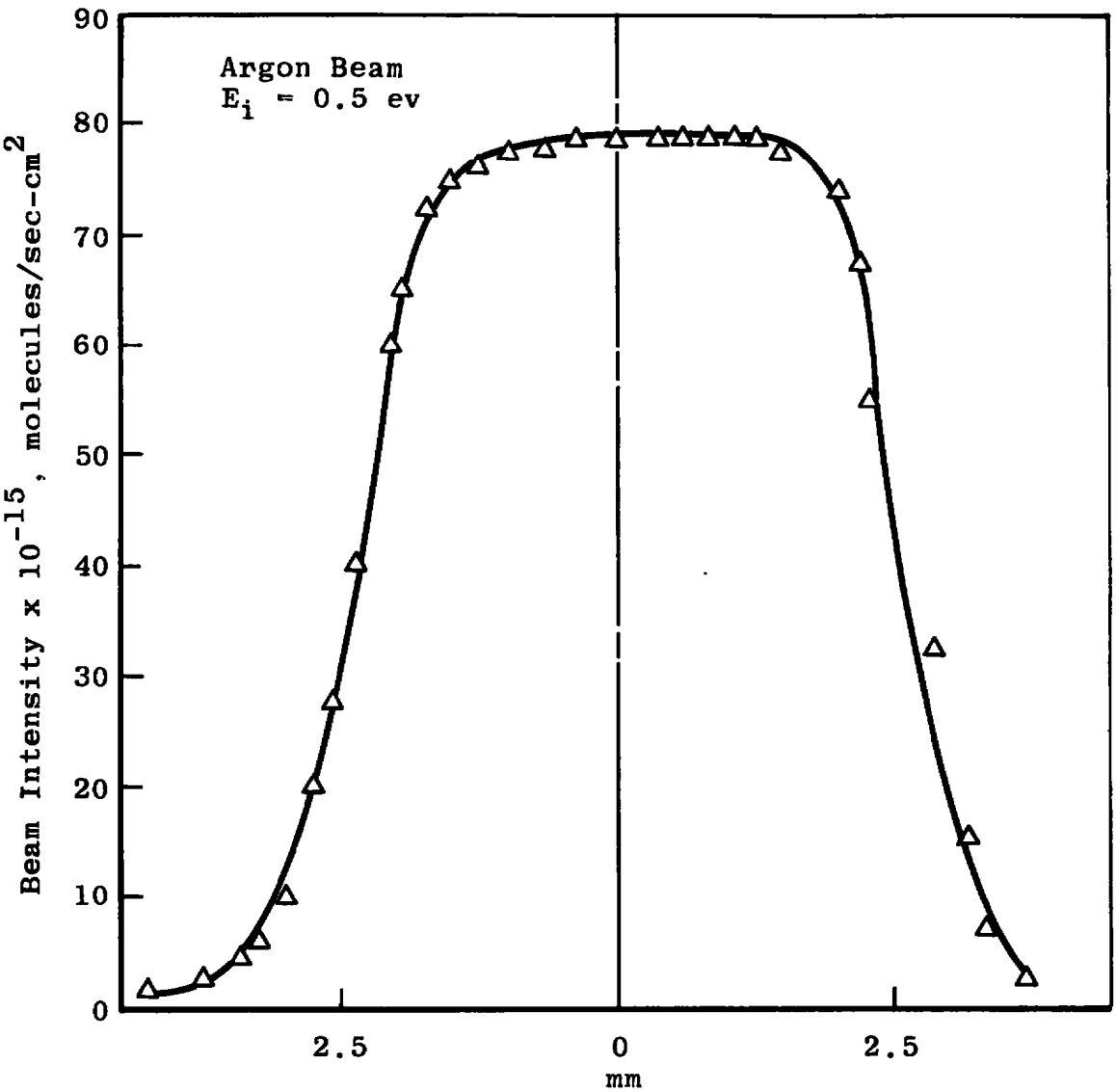

Fig. 9 Intensity Cross-Section of the Beam

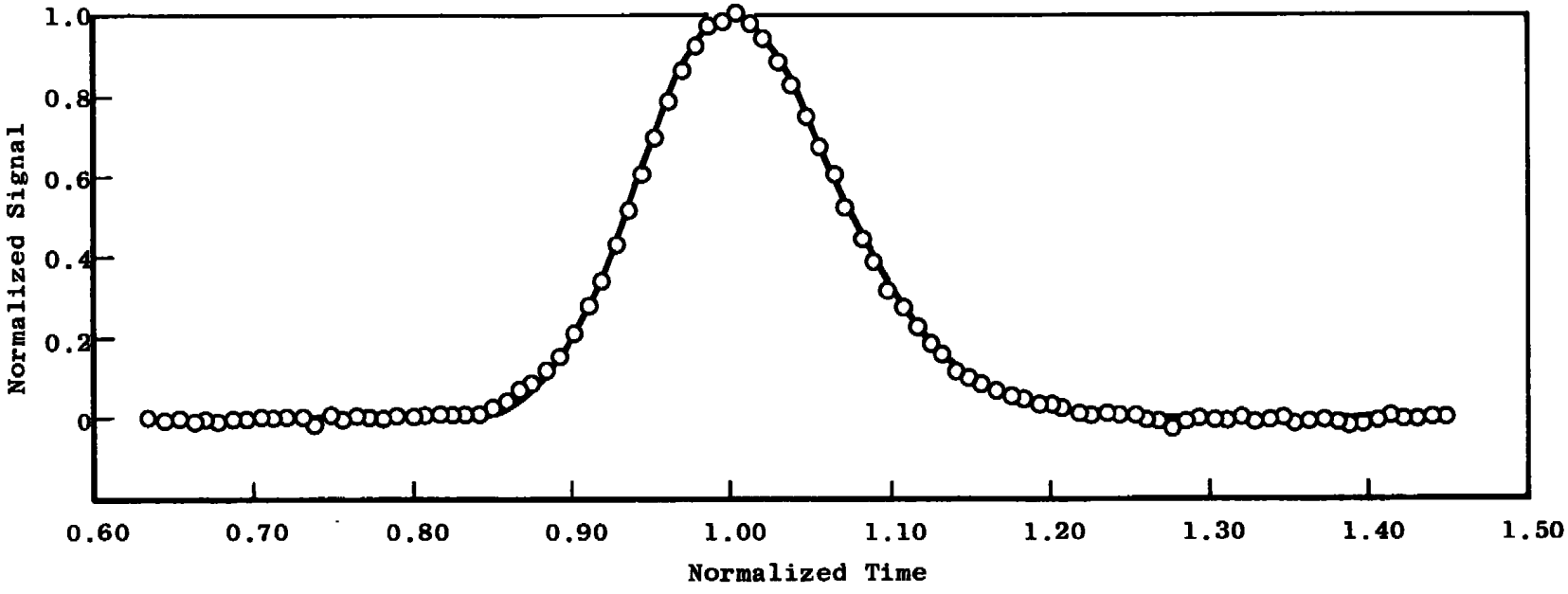

Fig. 10 Time-of-Flight Distribution of a 0.43-ev Argon Beam

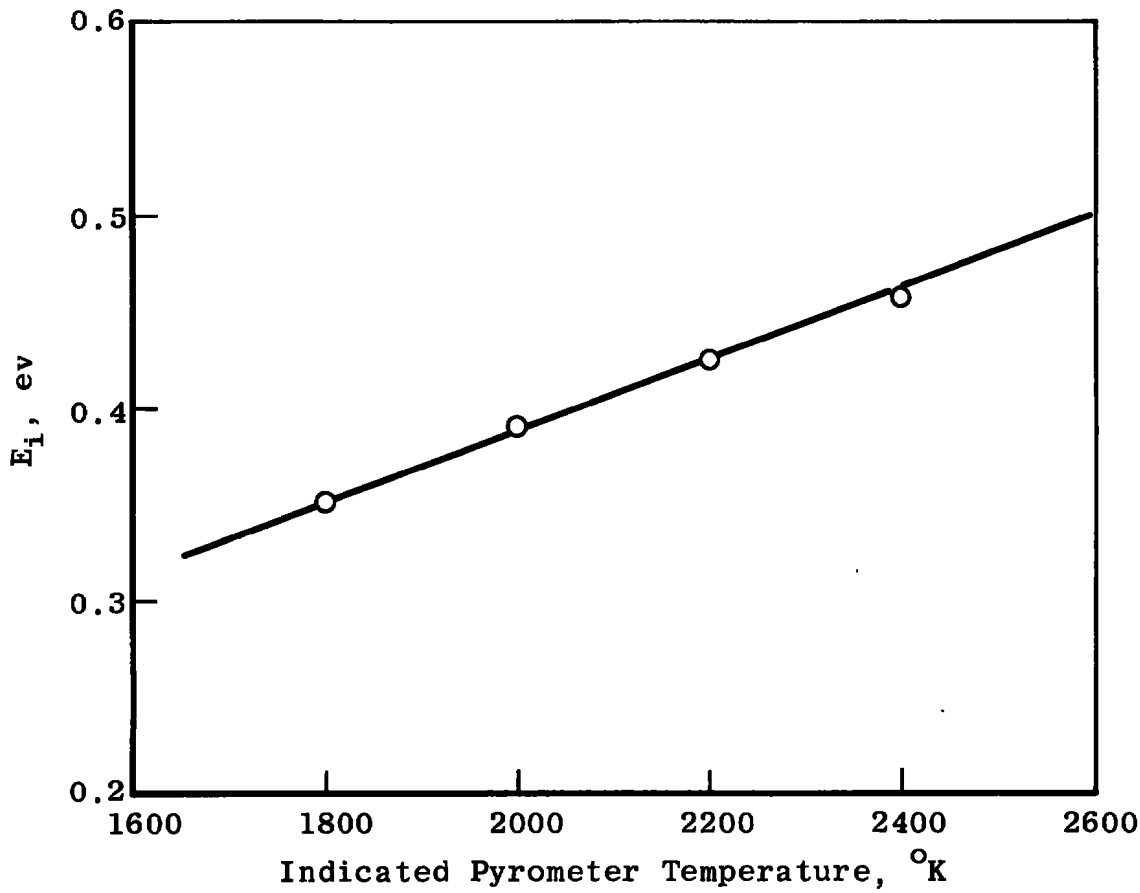

Fig. 11 Argon Beam Energy for Corresponding Source Temperatures

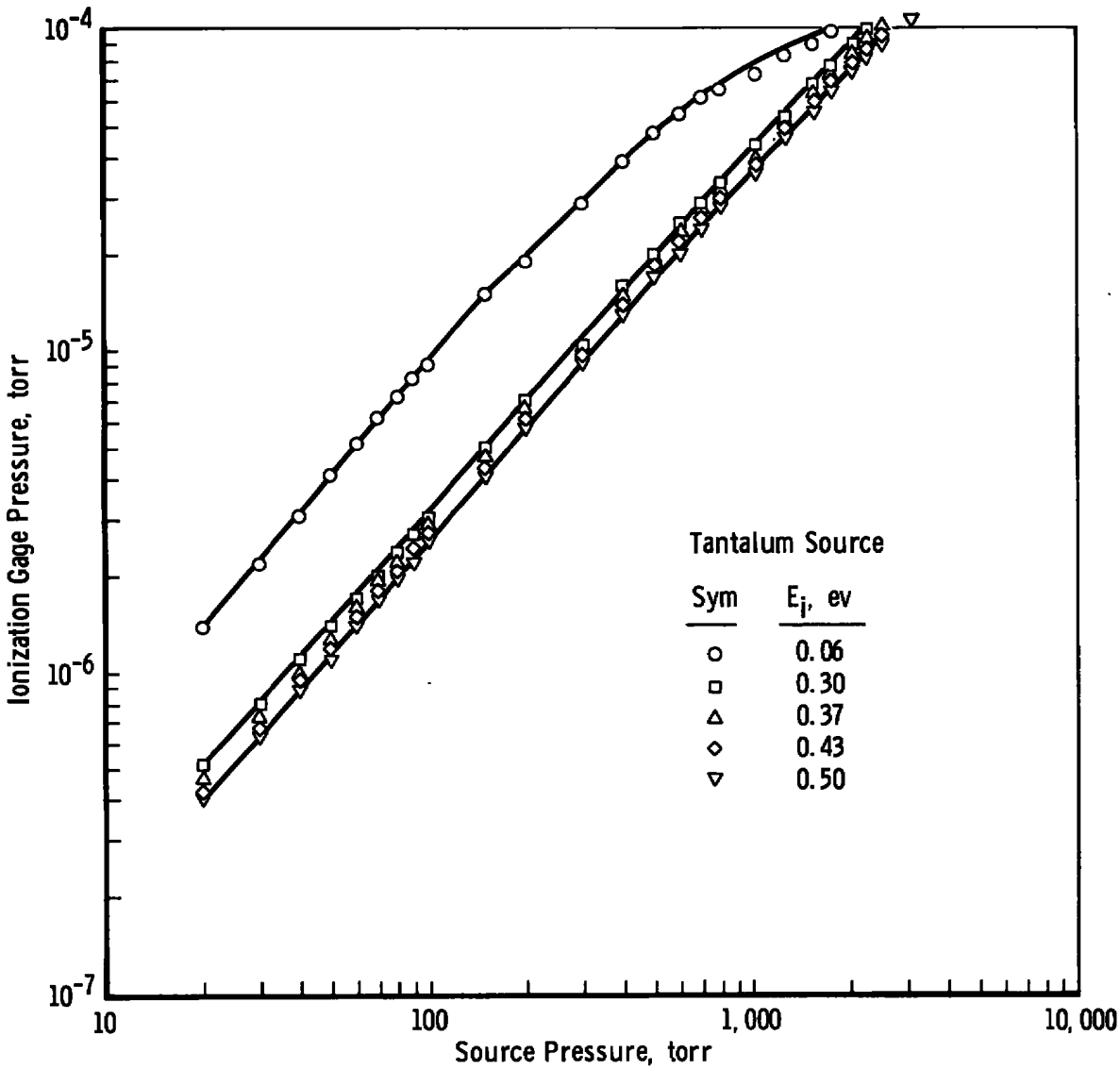

Fig. 12 Argon Beam Performance

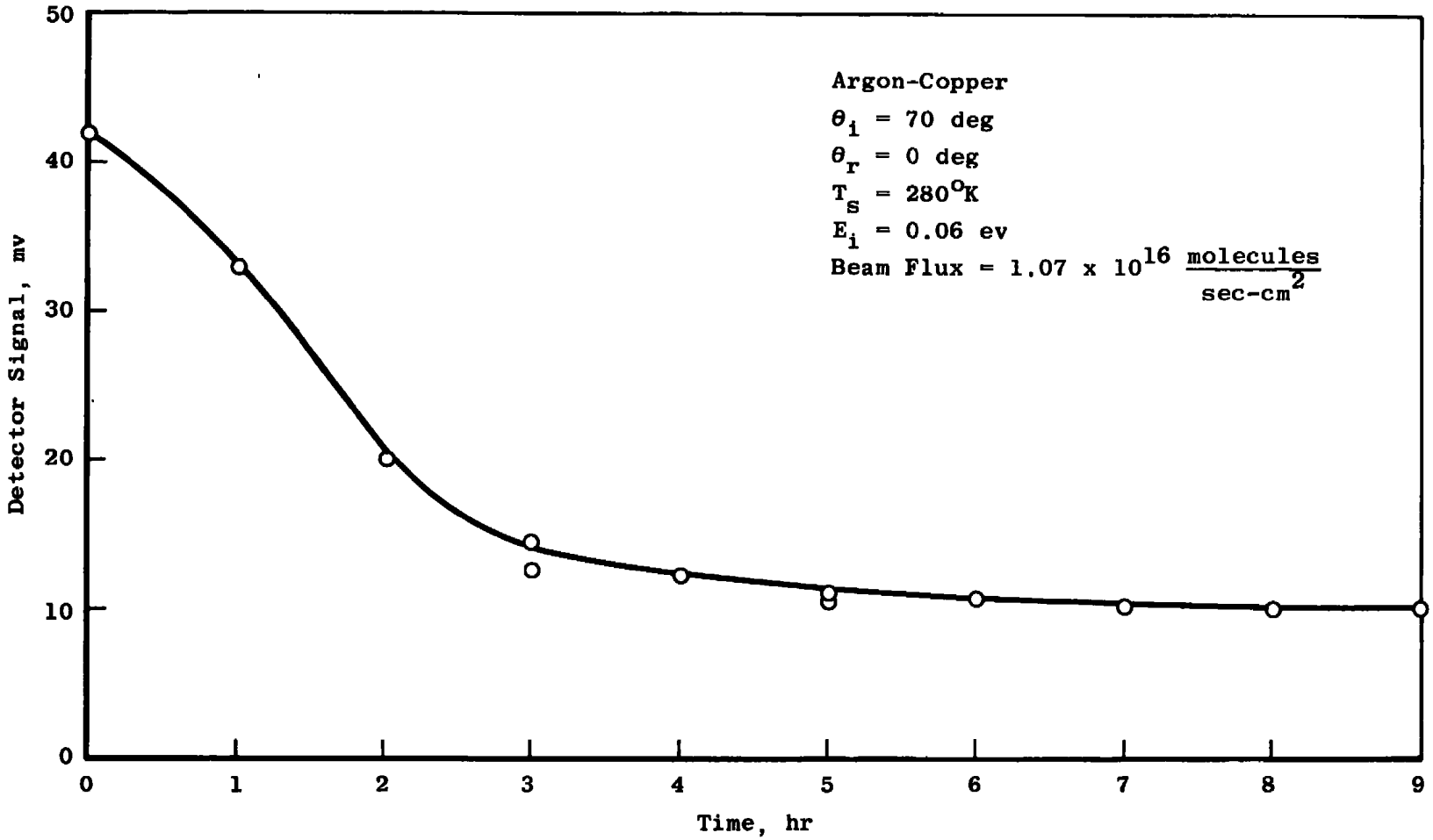

Fig. 13 Variation of Detector Sensitivity

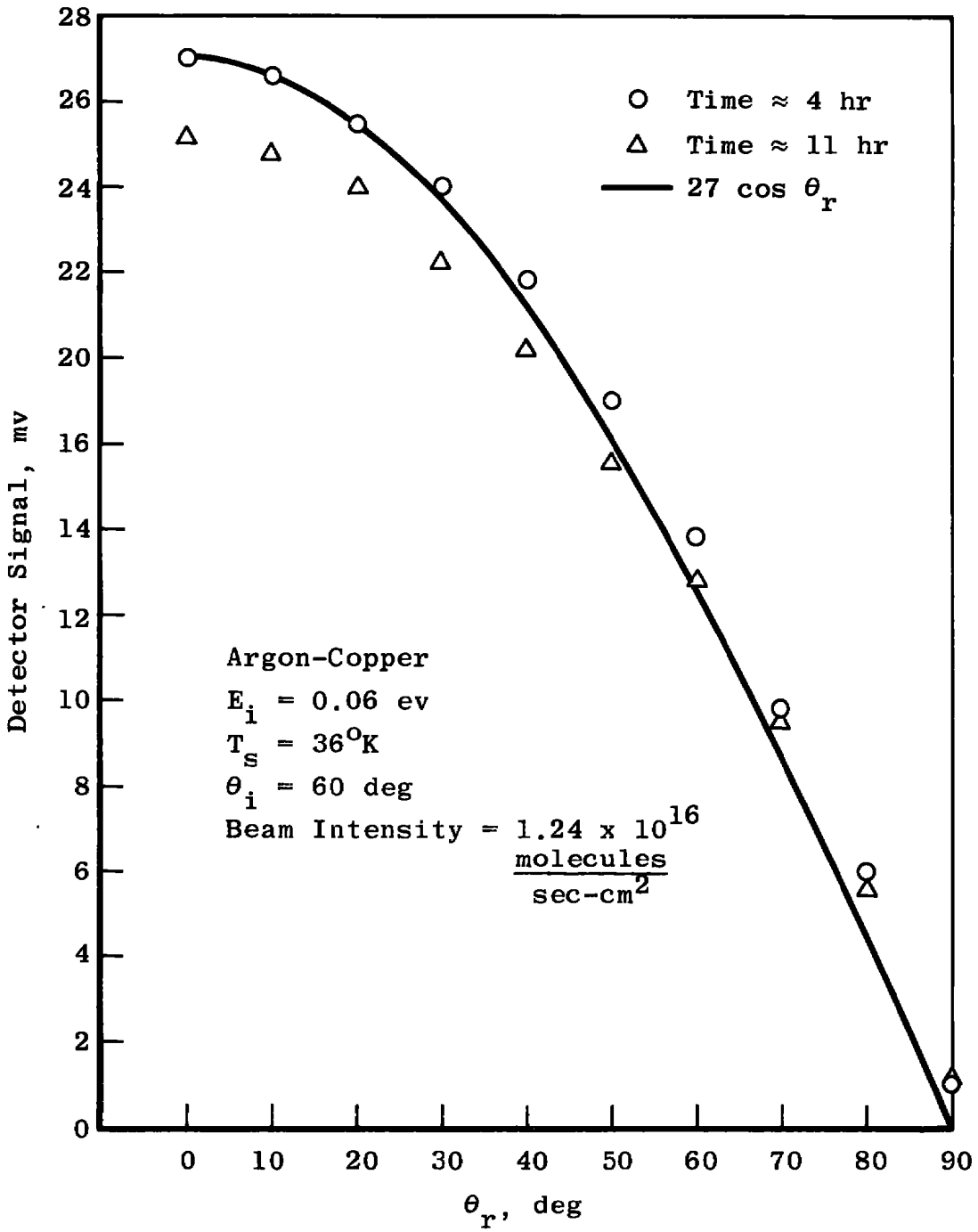

Fig. 14 Reference Cosine Spatial Distributions

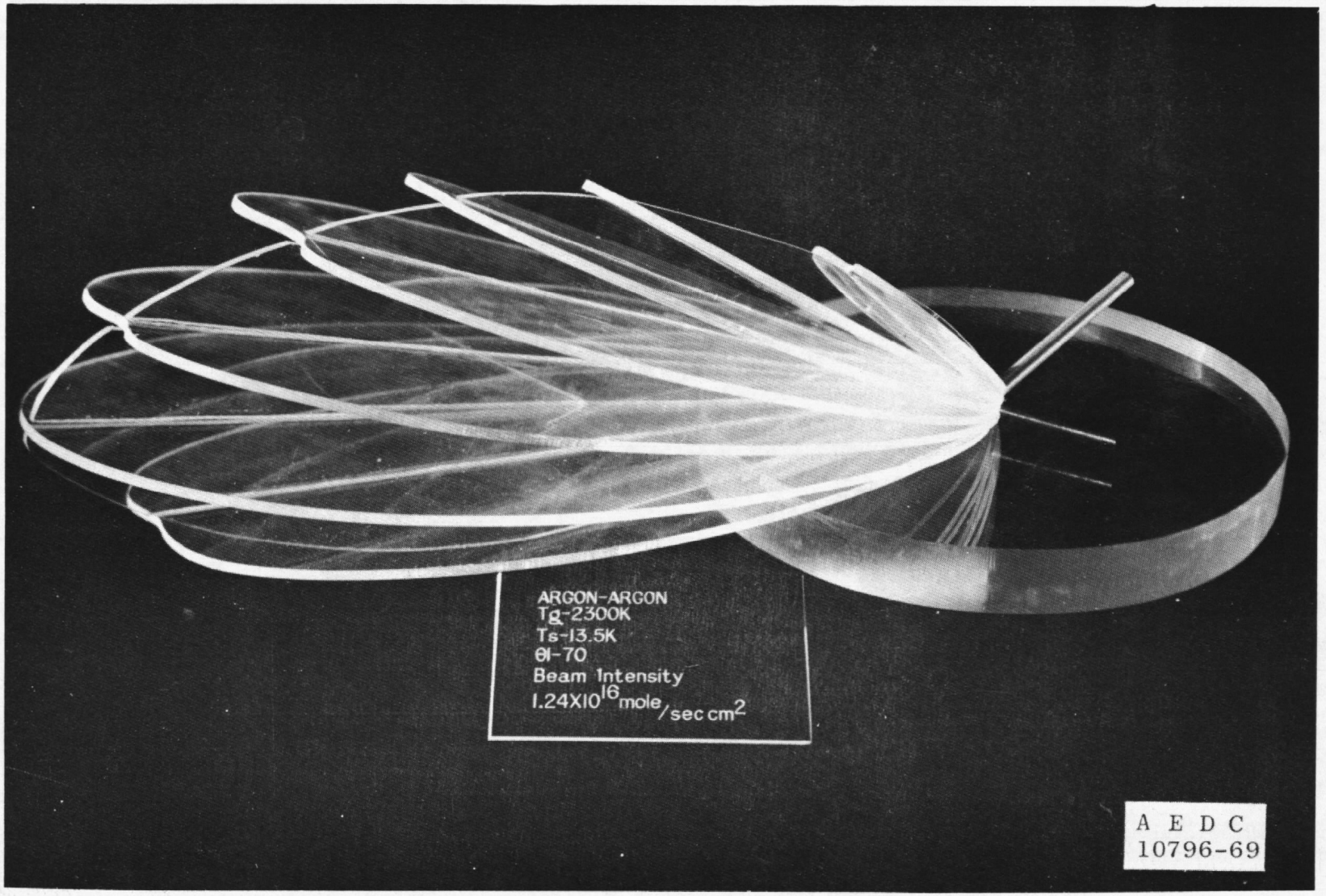

Fig. 15 Model of a Typical Scattering Distribution

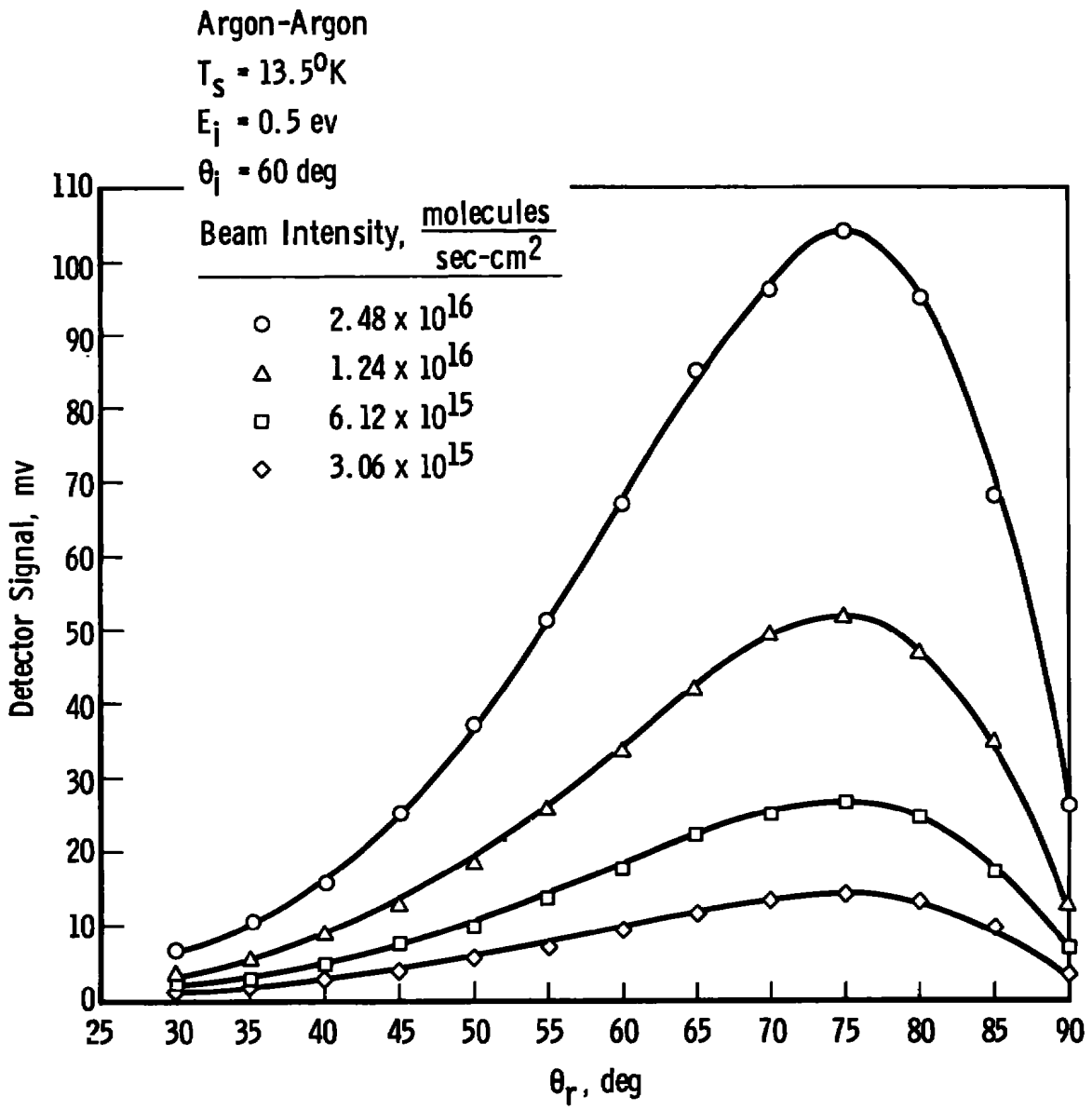

Fig. 16 In-Plane Scattering Distributions for Various Beam Intensities

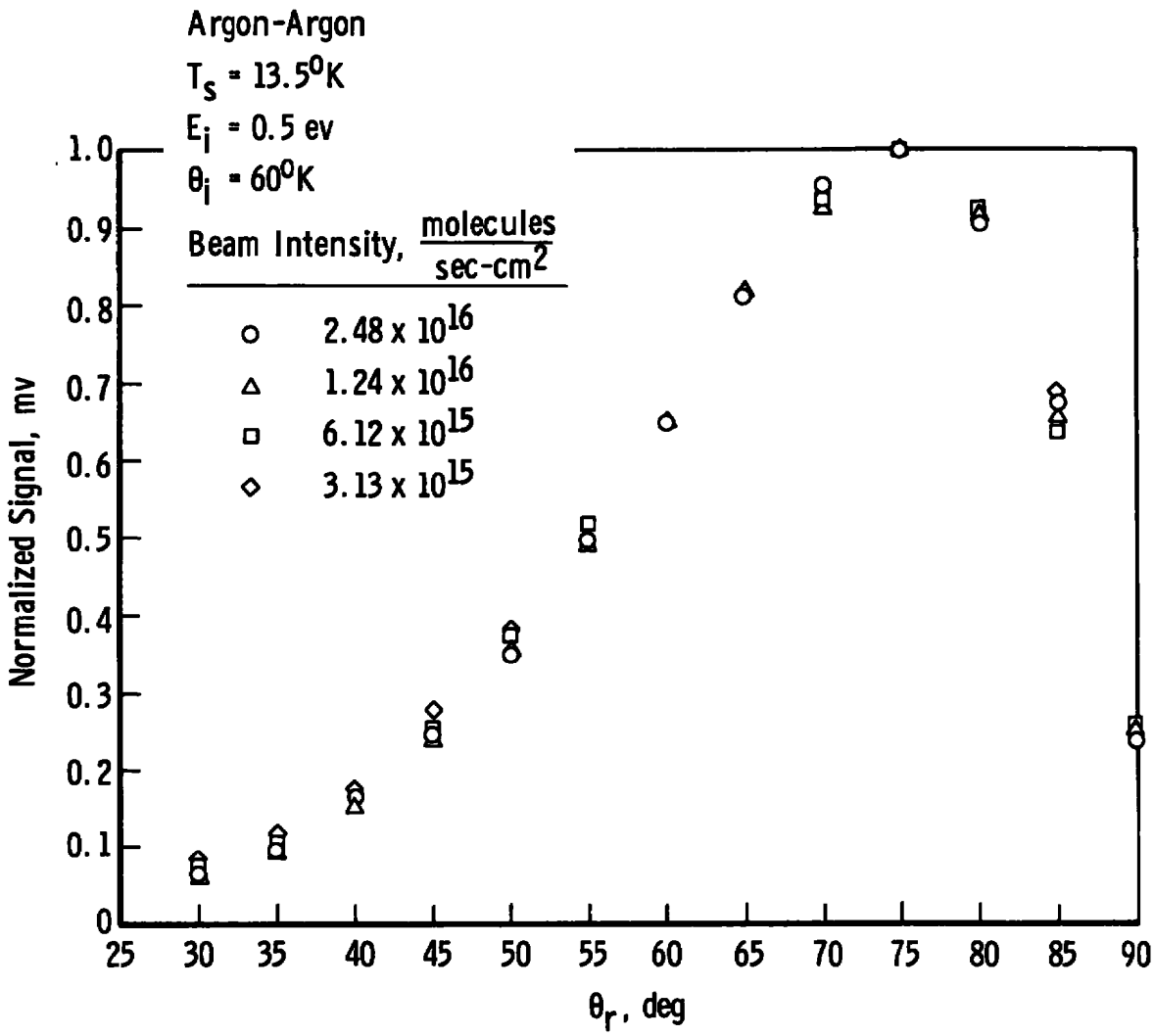

Fig. 17 Normalized In-Plane Scattering Distributions for Various Beam Intensities

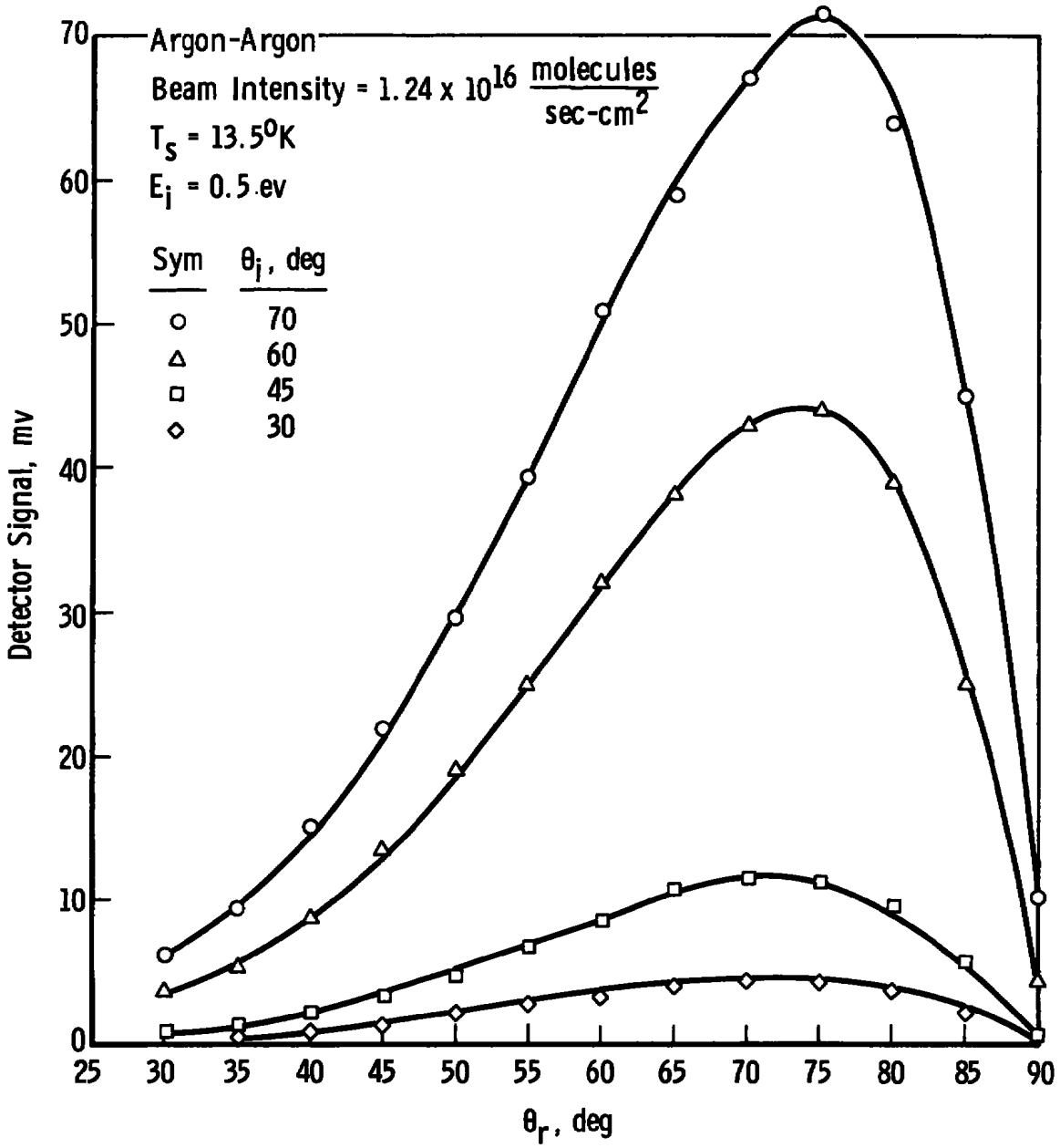

Fig. 18 In-Plane Scattering Distributions for Various Incidence Angles

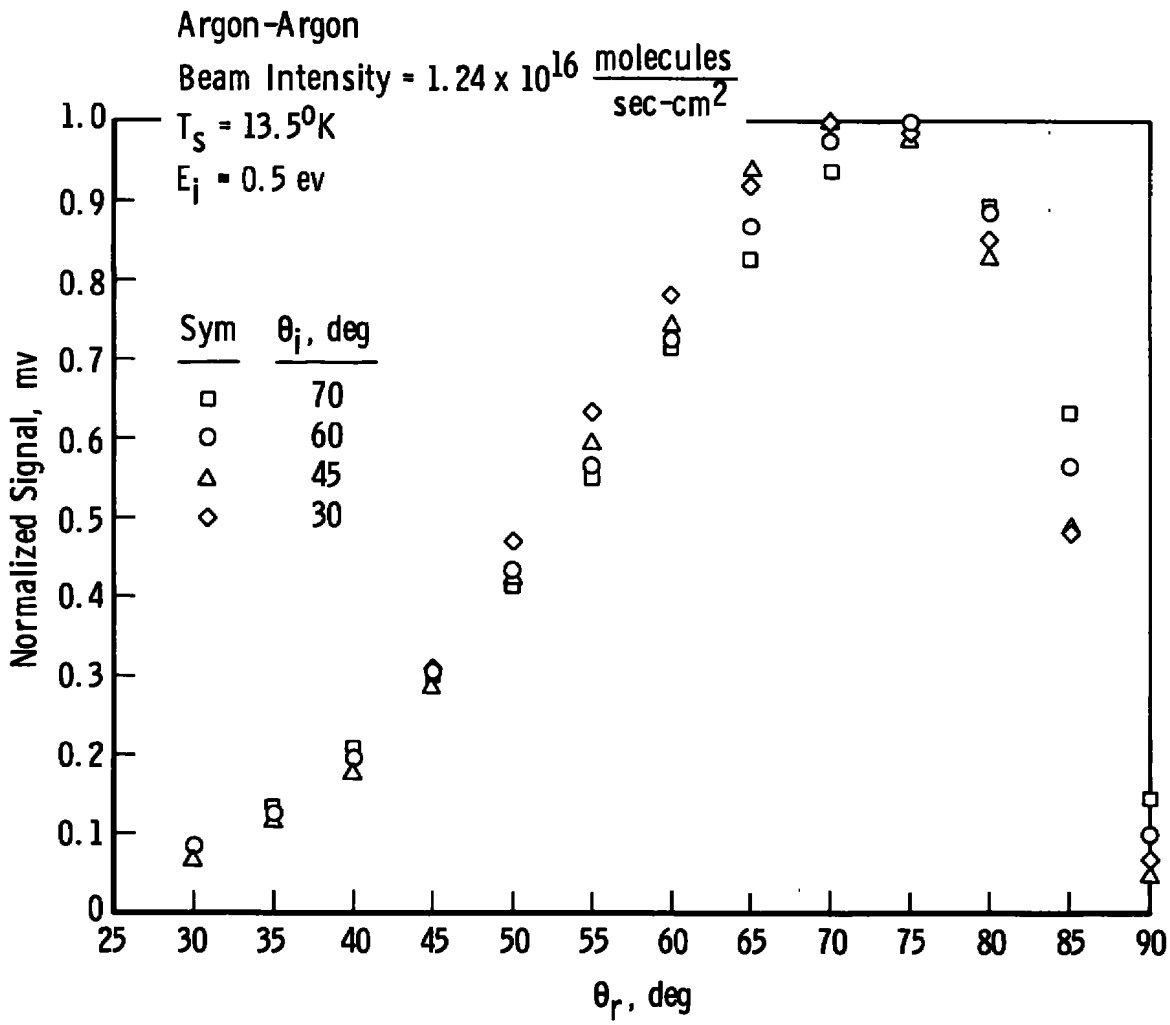

Fig. 19 Normalized In-Plane Scattering Distributions for Various Incidence Angles

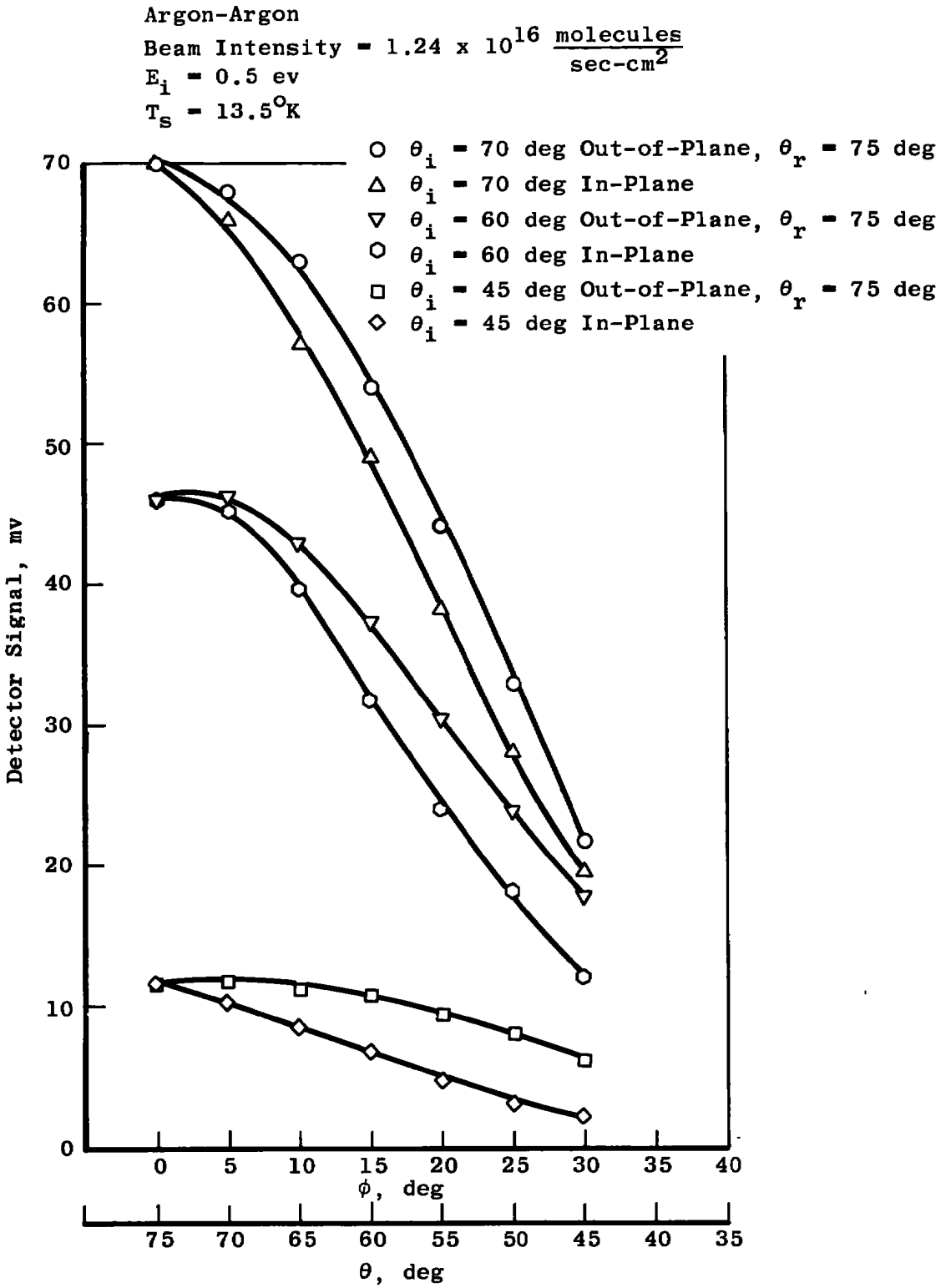

Fig. 20 Comparison of Out-of-Plane and In-Plane Scattering Distributions for Various Incidence Angles

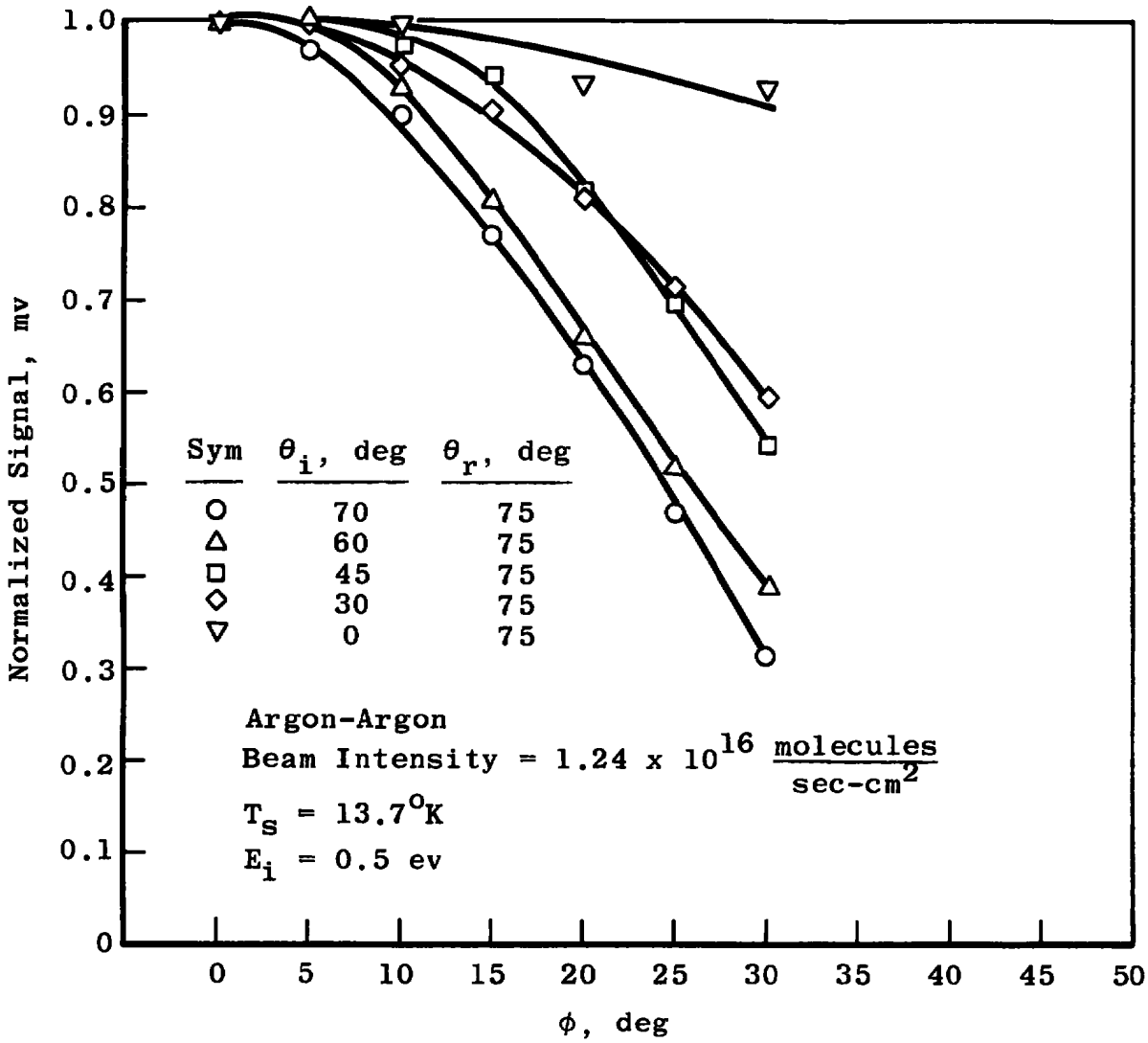

Fig. 21 Normalized Out-of-Plane Scattering Distributions for Various Incidence Angles

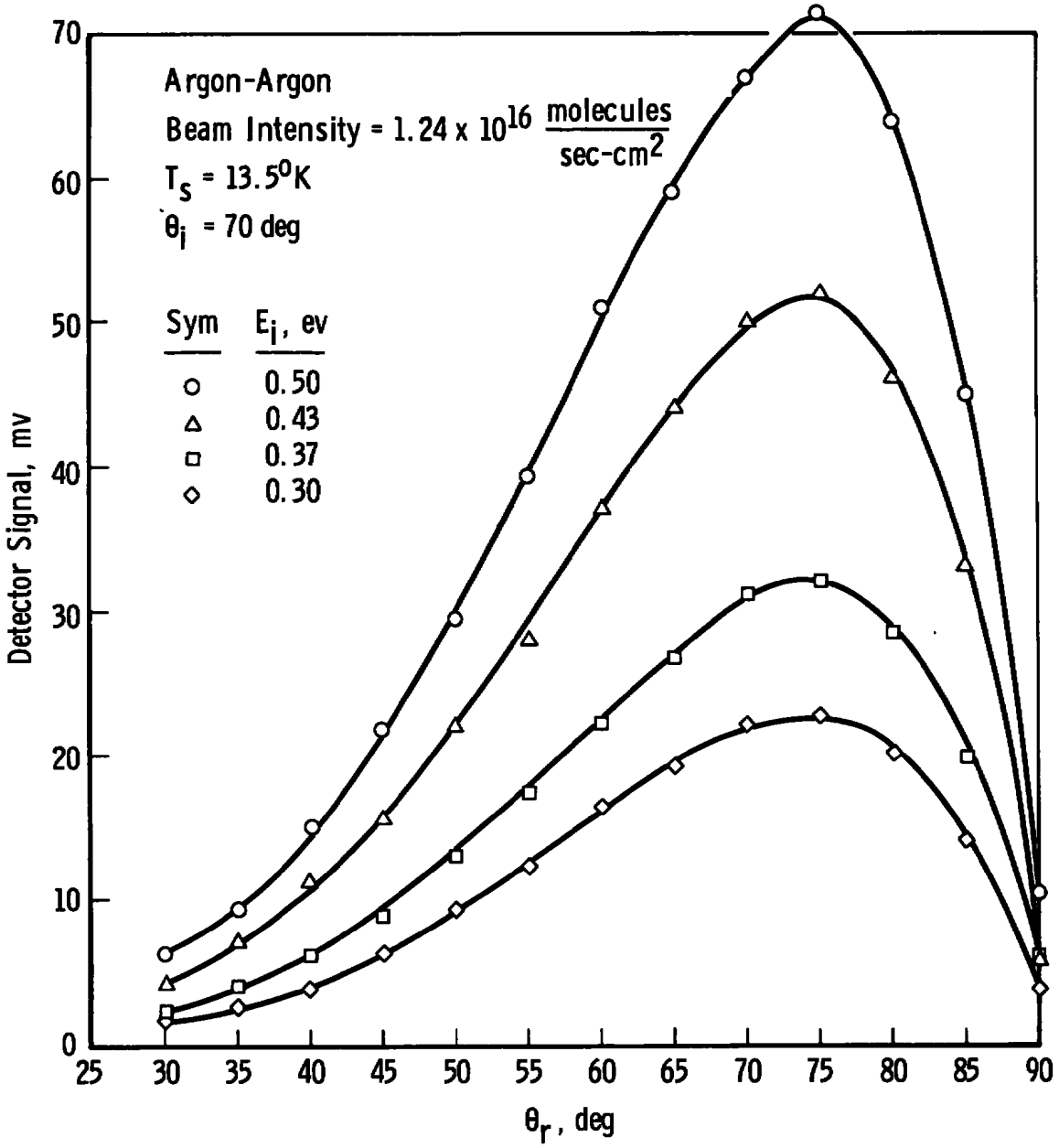

Fig. 22 In-Plane Scattering Distributions for Various Beam Energies (θ_i = 70 deg)

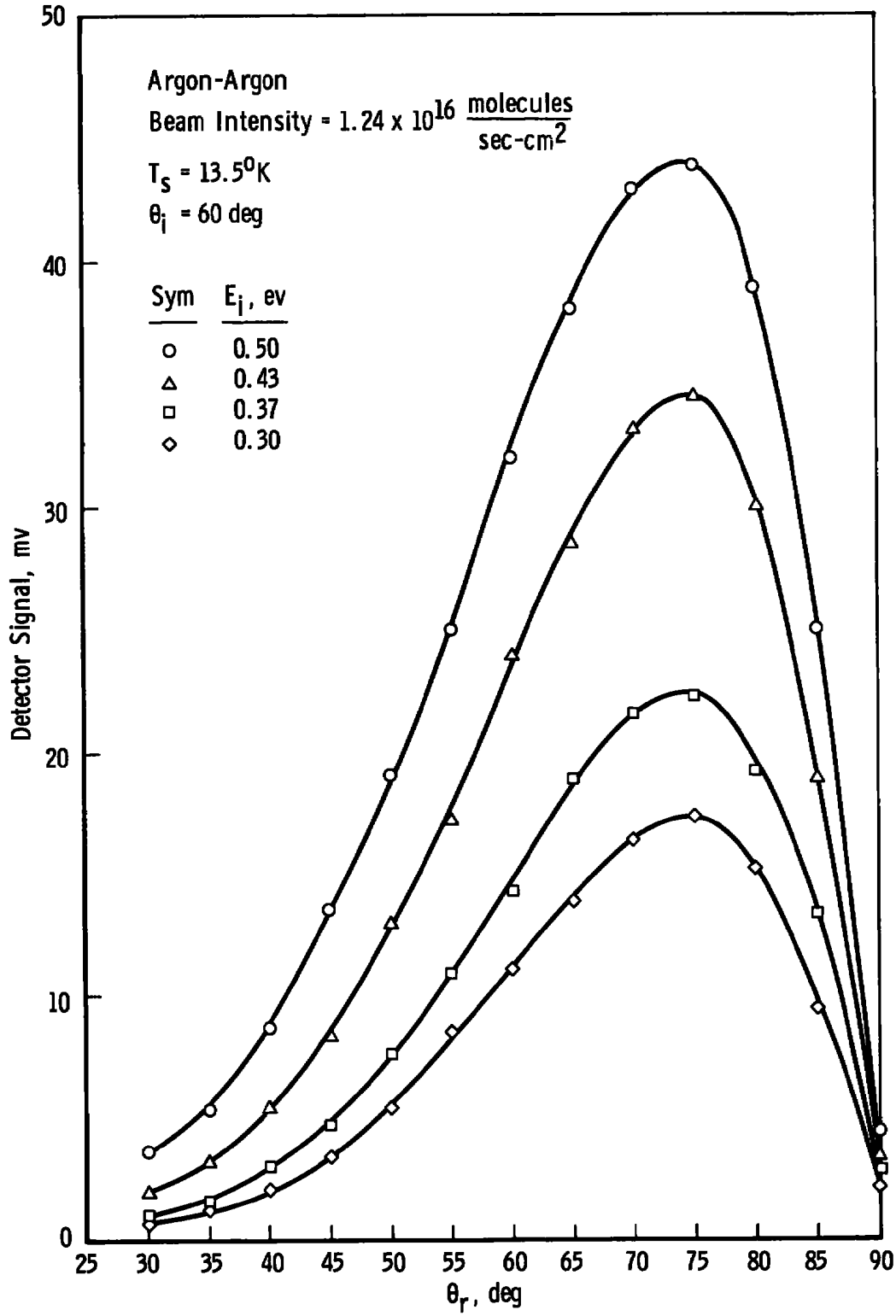

Fig. 23 In-Plane Scattering Distributions for Various Beam Energies (θ_i = 60 deg)

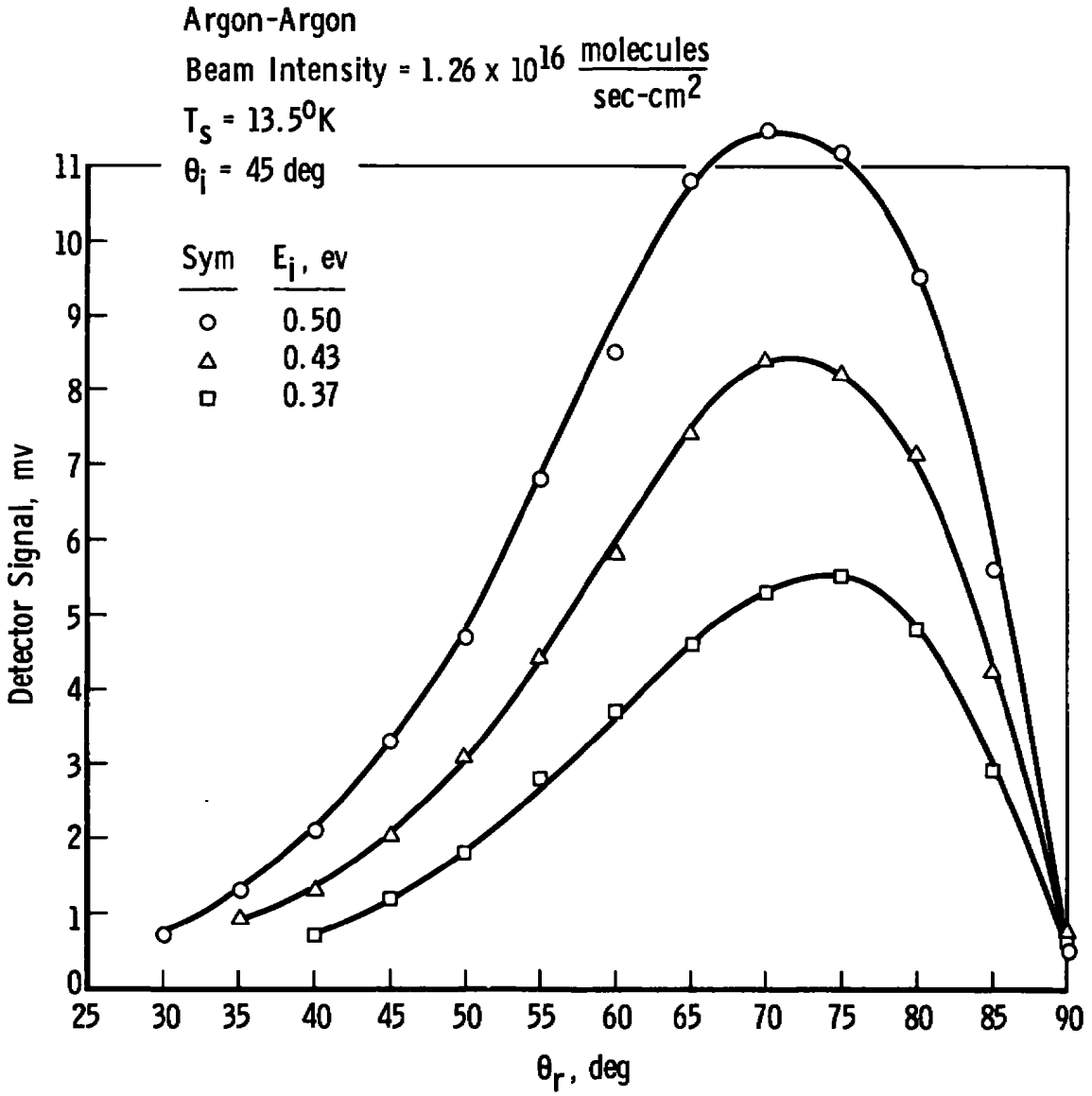

Fig. 24 In-Plane Scattering Distributions for Various Beam Energies (θ_i = 45 deg)

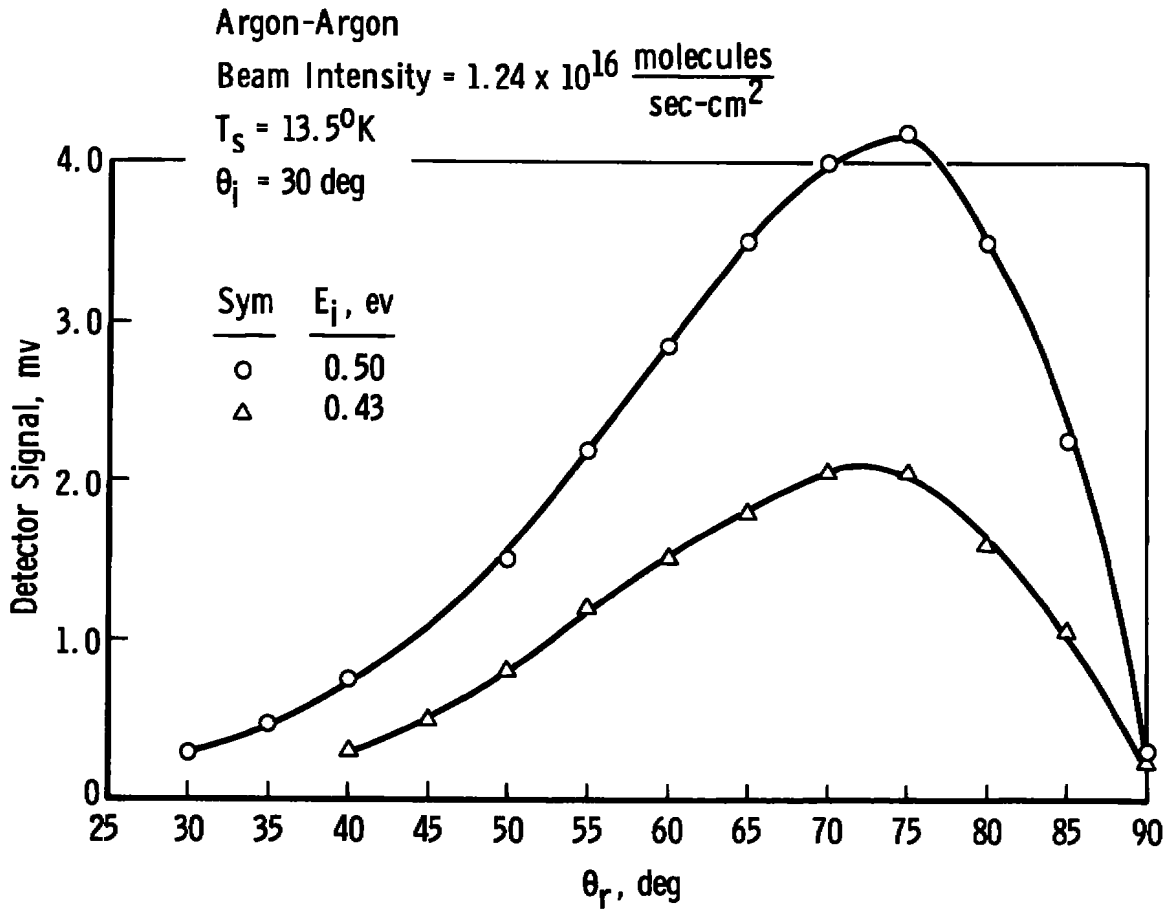

Fig. 25 In-Plane Scattering Distributions for Various Beam Energies (θ_i = 30 deg)

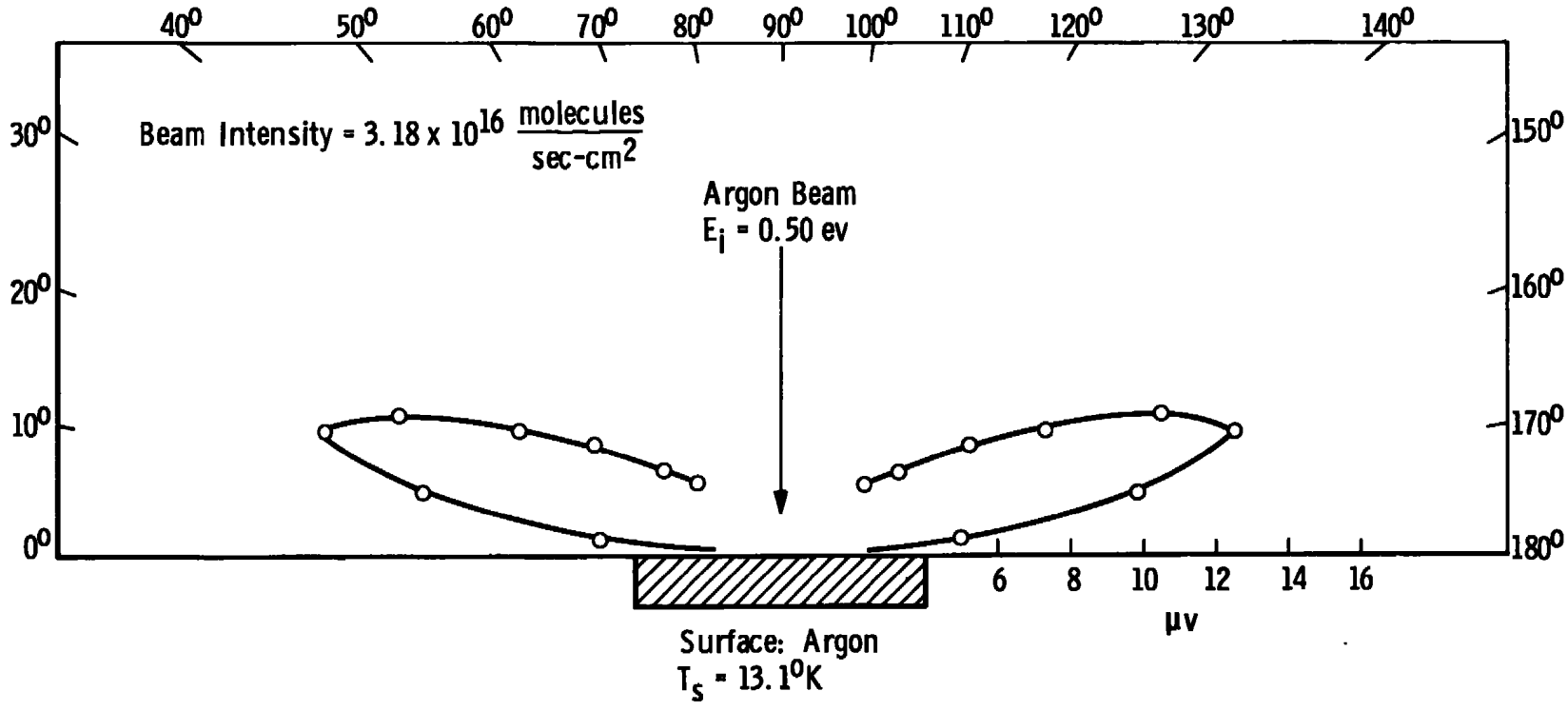

Fig. 26 In-Plane Scattering Distribution for a 0.5-ev Argon Beam at θ = 0 deg

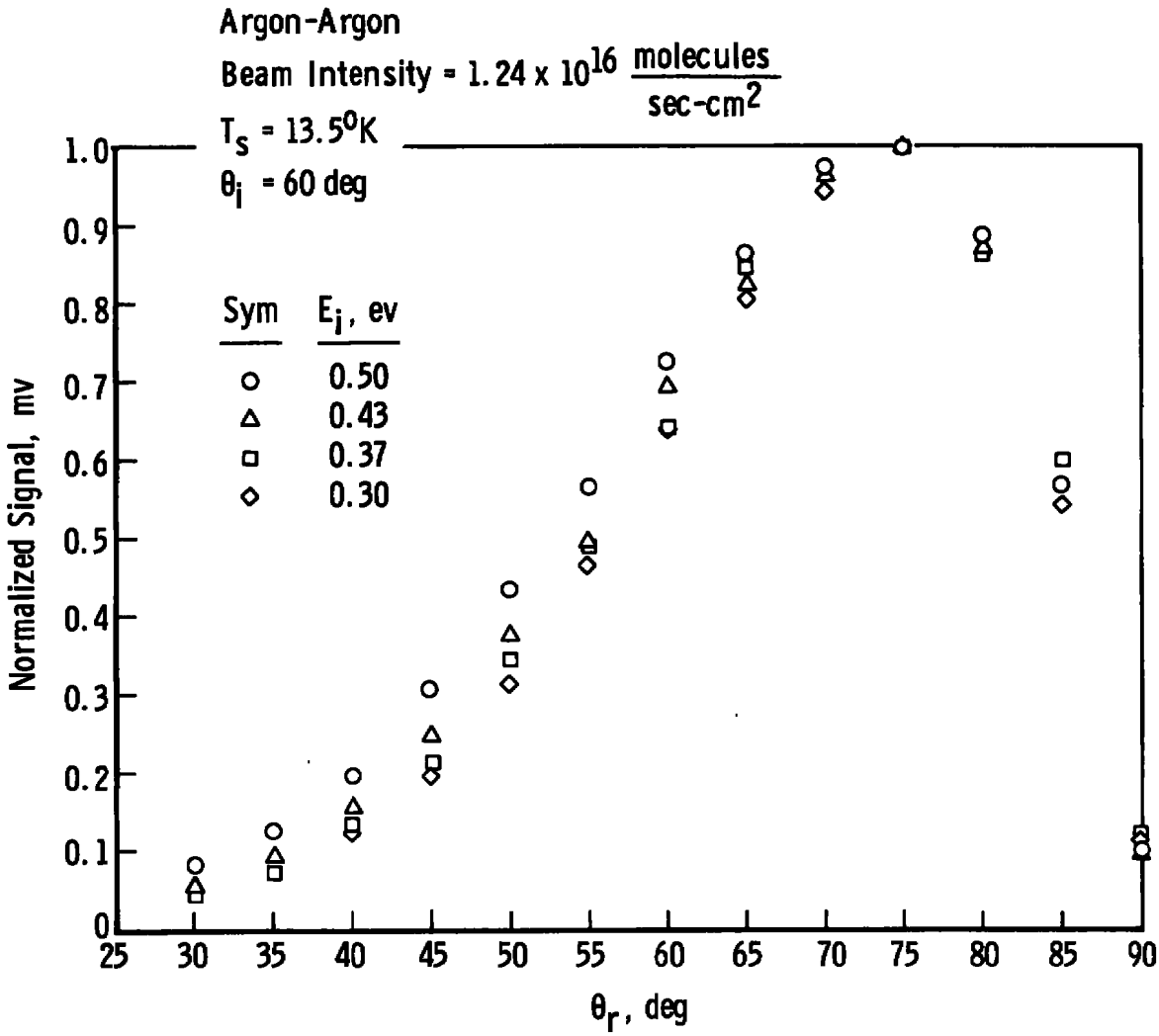

Fig. 27 Normalized In-Plane Scattering Distributions for Various Beam Energies (θ_i = 60 deg)

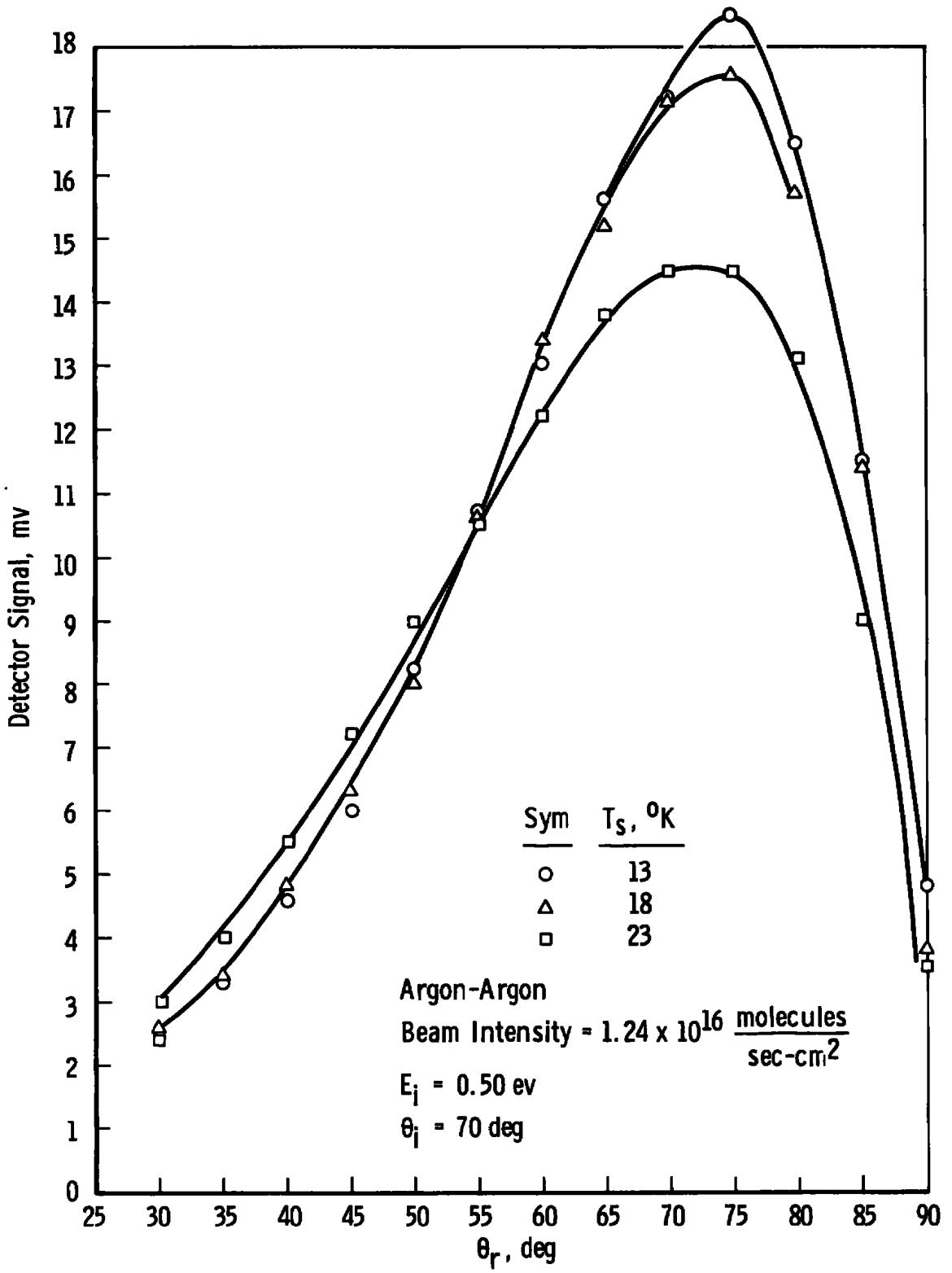

Fig. 28 In-Plane Scattering Distributions of a 0.5-ev Argon Beam at Various Surface Temperatures

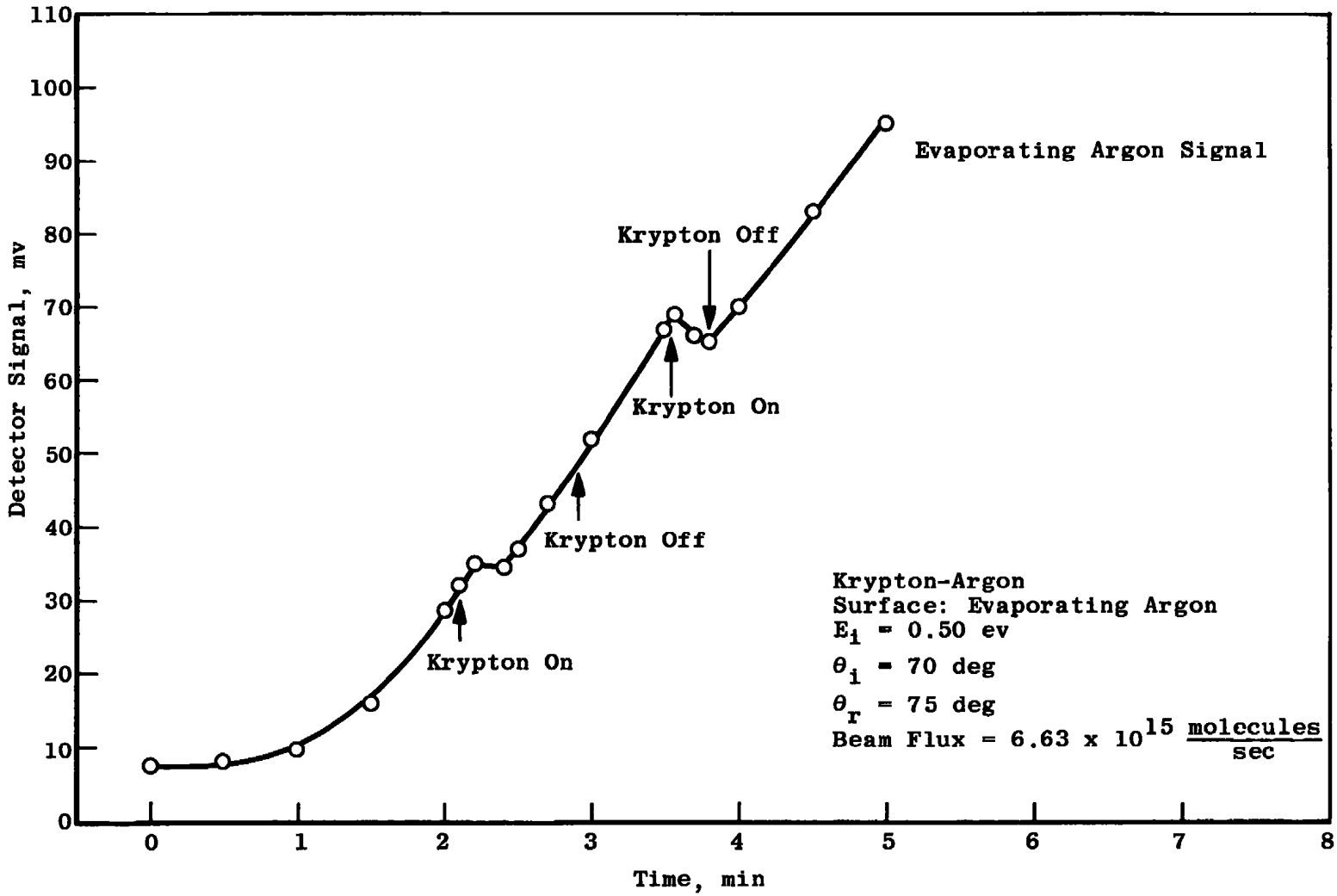

Fig. 29 Variation of Evaporating Argon Flux Due to an Impinging Krypton Beam

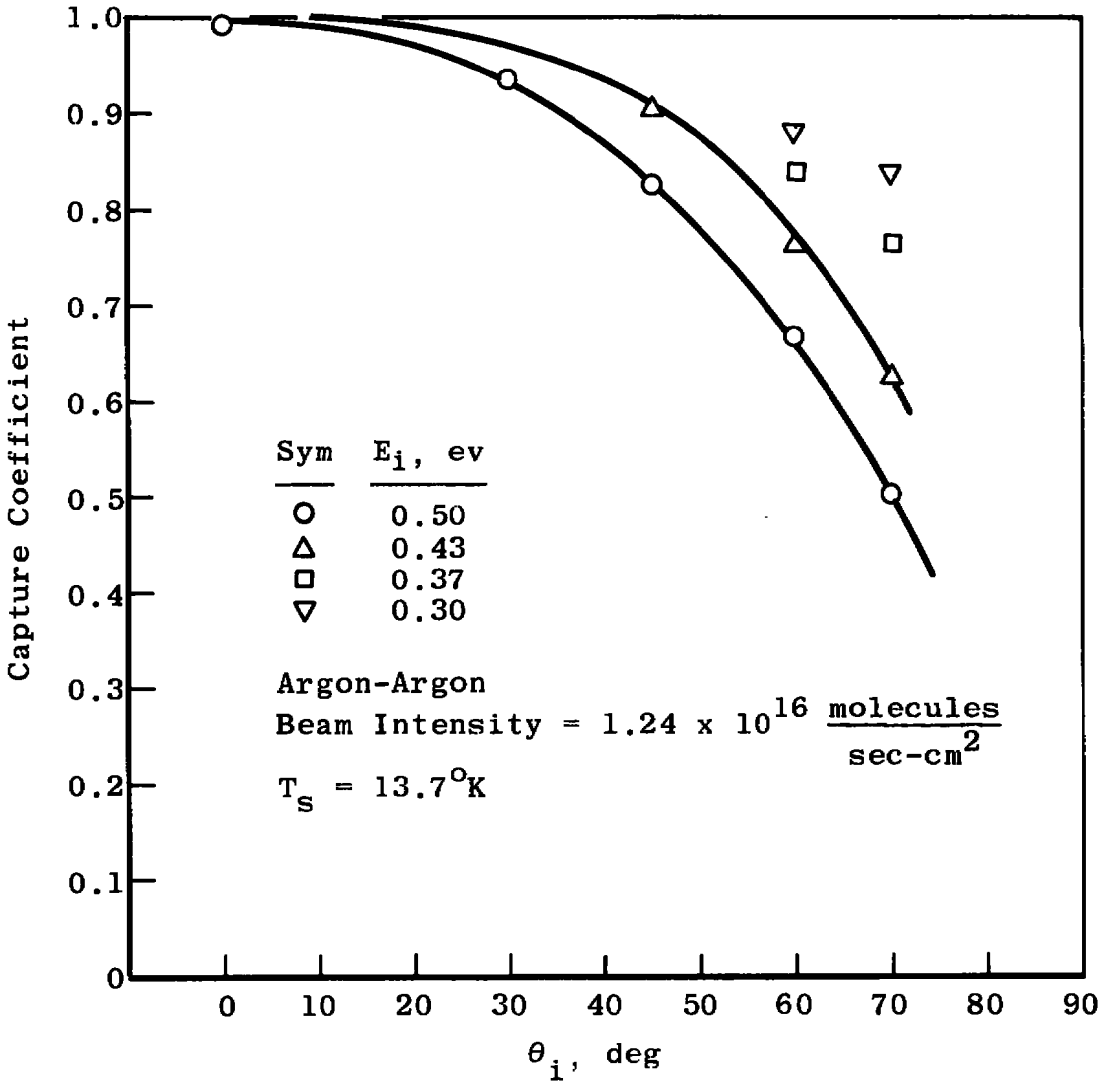

Fig. 30 Beam Capture Coefficient for Various Beam Incidence Angles

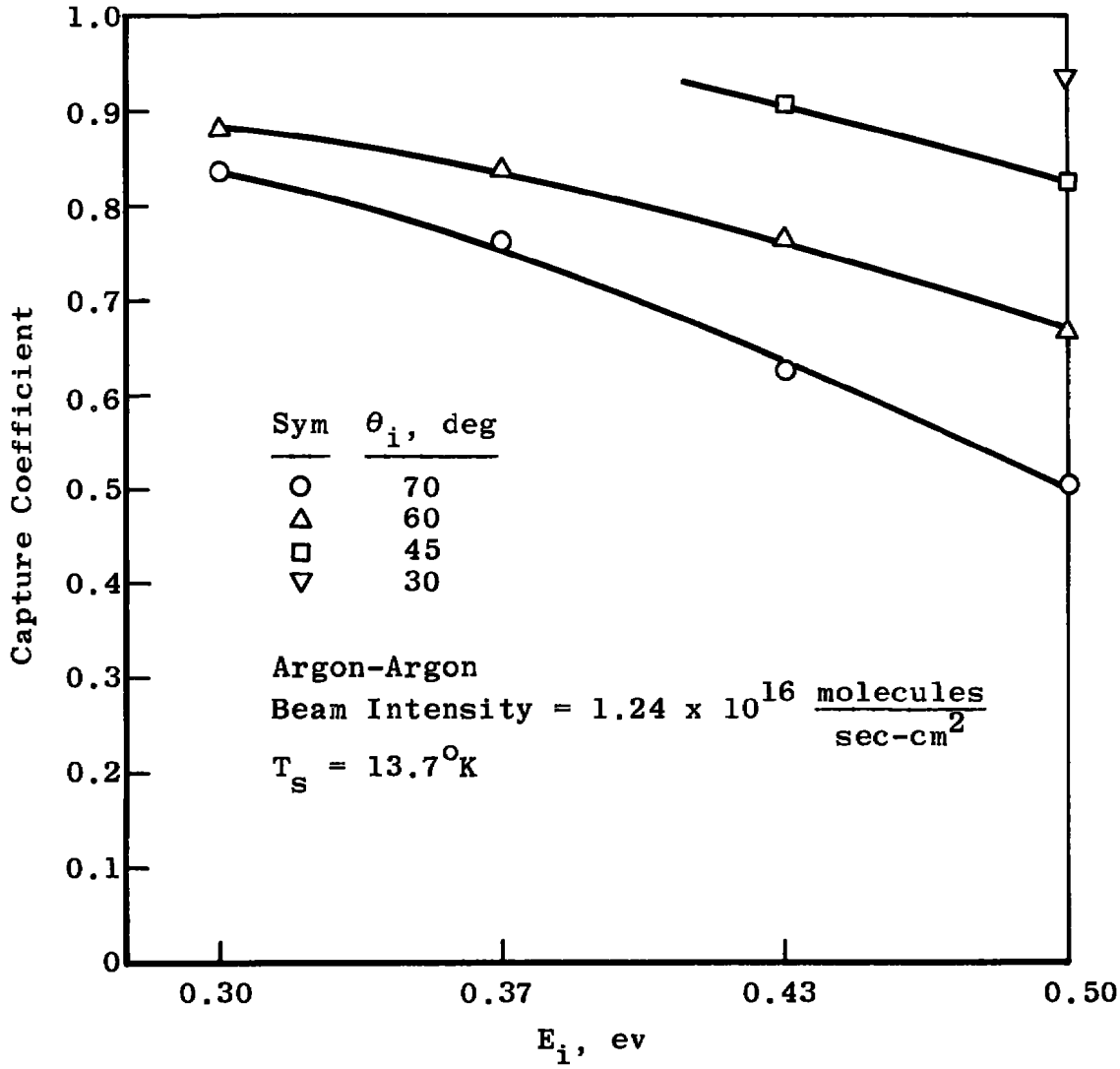

Fig. 31 Beam Capture Coefficient for Various Beam Incidence Energies

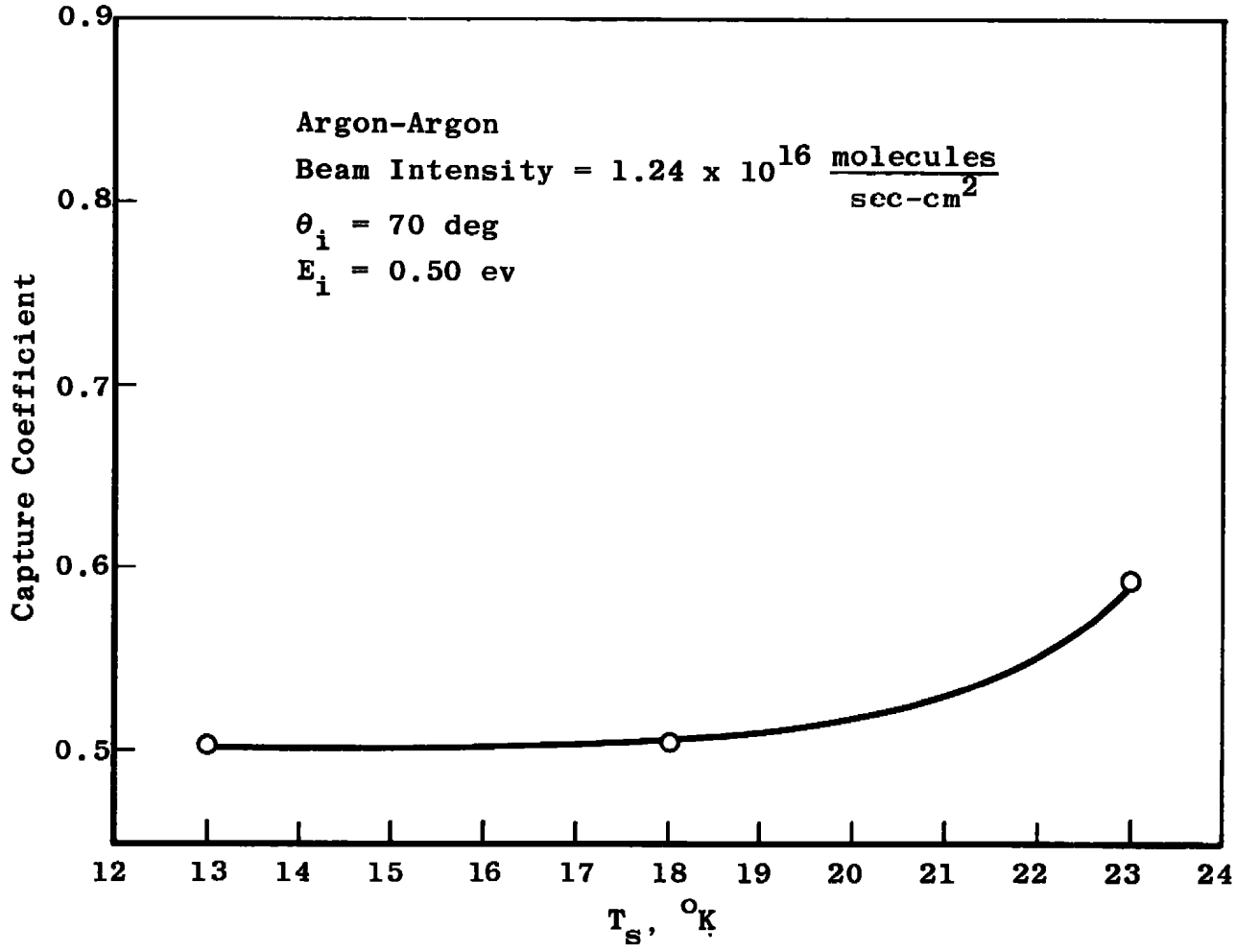

Fig. 32 Beam Capture Coefficient for Various Surface Temperatures

TABLE I
ARGON BEAM GAS ANALYSIS

Gas:	Matheson Gold Label Ultra-Pure Argon–Ionization Grade	
Purity:	99.999% minimum	
Analysis:	CO_2	~0.5 ppm
	O_2	1.5 ppm
	H_2	~1.0 ppm
	N_2	<5.0 ppm
	H_2O	<2.0 ppm
	CH_4	<0.4 ppm

UNCLASSIFIED

Security Classification

DOCUMENT CONTROL DATA - R & D

(Security classification of title, body of abstract and indexing annotation must be entered when the overall report is classified)

1. ORIGINATING ACTIVITY *(Corporate author)*
Arnold Engineering Development Center
ARO, Inc., Operating Contractor
Arnold Air Force Station, Tennessee

2a. REPORT SECURITY CLASSIFICATION
UNCLASSIFIED

2b. GROUP
N/A

3. REPORT TITLE
EXPERIMENTAL INVESTIGATION OF THE SCATTERING OF A MONOENERGETIC ARGON MOLECULAR BEAM FROM A SOLID ARGON SURFACE

4 DESCRIPTIVE NOTES *(Type of report and inclusive dates)*
November to December 1969 - Final Report

5. AUTHOR(S) *(First name, middle initial, last name)*
M. R. Busby and R. F. Brown, ARO, Inc.

6. REPORT DATE	7a. TOTAL NO. OF PAGES	7b. NO. OF REFS
October 1970	58	25

8a. CONTRACT OR GRANT NO.
F40600-71-C-0002

b. PROJECT NO.

c. Program Element 61102F

d.

9a. ORIGINATOR'S REPORT NUMBER(S)
AEDC-TR-70-90

9b. OTHER REPORT NO(S) *(Any other numbers that may be assigned this report)*
ARO-VKF-TR-70-90

10 DISTRIBUTION STATEMENT
This document has been approved for public release and sale; its distribution is unlimited.

11. SUPPLEMENTARY NOTES
Available in DDC

12. SPONSORING MILITARY ACTIVITY
Arnold Engineering Development Center, Air Force Systems Command
Arnold AF Station, Tennessee 37389

13. ABSTRACT An aerodynamic molecular beam and phase sensitive detection system were used to investigate the spatial distributions of argon atoms scattered from solid argon for: incident beam energies of 0.3 (T_o = 1400 °K), 0.37 (1700°K), 0.43 (2000°K), and 0.5 ev (2300°K); incident angles (measured with respect to the surface normal) of 0 to 70 deg; and solid argon temperatures of 13.5°K. The effect of surface temperature on the distributions for 0.5-ev beams at 70-deg incidence was studied in the range from 13.5 to 23°K. Both in-plane and out-of-plane spatial distribution measurements were made, and highly nondiffuse supraspecular flux distributions were observed for the noncondensing atoms. The experimental data indicated that the angle of maximum reflected intensity was independent of the beam intensities, beam energies, beam incidence angles, and surface temperatures investigated; and its value was approximately 75 deg. The shape of the in-plane spatial distributions was essentially independent of the beam incidence angles and beam intensities studied. However, for increasing beam energies, the scattering distributions broadened. The out-of-plane distributions were broader than the corresponding in-plane lobes. The beam capture coefficient was a monotonically decreasing function as the angle of incidence and the incident beam energy increased. However, the capture coefficient of a 0.5-ev argon beam impinging at 70 deg increased as the surface temperature increased from 13 to 23°K.

DD FORM 1 NOV 65 1473

UNCLASSIFIED

Security Classification

14 KEY WORDS	LINK A		LINK B		LINK C	
	ROLE	WT	ROLE	WT	ROLE	WT
argon						
molecular beams						
scattering						
spatial distribution						
interactions						